Journal Pre-proofs

Molecular Heterogeneity in Pyrogenic Dissolved Organic Matter From A Thermal Series of Oak and Grass Chars

Andrew S. Wozniak, Aleksandar I. Goranov, Siddhartha Mitra, Kyle W. Bostick, Andrew R. Zimmerman, Danielle R. Schlesinger, Satish Myneni, Patrick G. Hatcher

PII: S0146-6380(20)30100-5
DOI: https://doi.org/10.1016/j.orggeochem.2020.104065
Reference: OG 104065

To appear in: *Organic Geochemistry*

Received Date: 28 February 2020
Revised Date: 15 June 2020
Accepted Date: 19 June 2020

Please cite this article as: Wozniak, A.S., Goranov, A.I., Mitra, S., Bostick, K.W., Zimmerman, A.R., Schlesinger, D.R., Myneni, S., Hatcher, P.G., Molecular Heterogeneity in Pyrogenic Dissolved Organic Matter From A Thermal Series of Oak and Grass Chars, *Organic Geochemistry* (2020), doi: https://doi.org/10.1016/j.orggeochem.2020.104065

MOLECULAR HETEROGENEITY IN PYROGENIC DISSOLVED ORGANIC MATTER FROM A THERMAL SERIES OF OAK AND GRASS CHARS

Andrew S. Wozniak[a*], Aleksandar I. Goranov[b], Siddhartha Mitra[c], Kyle W. Bostick[d], Andrew R. Zimmerman[d], Danielle R. Schlesinger[e], Satish Myneni[e], Patrick G. Hatcher[b]

[1]School of Marine Science and Policy, University of Delaware, 1044 College Drive, Lewes, DE, 19958, USA, awozniak@udel.edu

[b]Department of Chemistry and Biochemistry, Old Dominion University, [c]Department of Geological Sciences, East Carolina University, [d]Department of Geological Sciences, University of Florida, [e]Department of Geosciences, Princeton University

*Corresponding Author:

ABSTRACT

Pyrogenic organic matter (Py-OM) generated via the incomplete combustion of biomass is well studied due to the presence of slow-cycling, condensed aromatic compounds (ConAC) known to sequester in soils and sediments. Recently, dissolved Py-OM (Py-DOM) has received interest due to its higher mobility and potential to be transferred through watersheds to aquatic systems. Py-DOM quantities, molecular identities, and importance to global carbon budgets and cycles are only beginning to be understood. Fourier transform ion cyclotron resonance mass spectrometry (FTICR-MS) analyses were performed on Py-DOM isolated from oak and grass biochars over a range of temperatures (250- 650°C), and the data are compared to complementary ^{1}H NMR spectroscopic and benzenepolycarboxylic acid biomarker (BPCAs) analyses. Py-DOM is revealed to be a heterogeneous mixture of compounds ranging in relative aromaticity and oxygenation. FTICR-MS analyses demonstrate a decrease in Py-DOM relative oxygen content

and a concurrent increase in aliphatic character and heteroatomic (N, Cl) content. ^{1}H NMR and BPCAs analyses detail low O/C dissolved ConAC not observed by FTICR-MS demonstrating the necessity for a multiple proxy approach to Py-DOM characterization. Heterogeneous Py-DOM is explained as resulting from pyrolysis-initiated and radical-mediated functional group cleavage, aromatic condensation, and aromatic ring-opening reactions. Oak biomass progresses faster along a char maturity continuum for a given pyrolysis temperature, perhaps due to its greater lignin content or radical quenching by grass cuticular material. Biomass species and pyrolysis temperature likely result in different Py-DOM compositions and fates and must be considered when evaluating the impacts of wildfires and biochar applications.

HIGHLIGHTS

- Pyrogenic dissolved organic matter (Py-DOM) is molecularly heterogeneous.
- Complementary analyses are needed to representatively characterize Py-DOM composition.
- Py-DOM becomes less oxygenated, more aromatic, and more aliphatic with increased char maturity.
- Grass and oak pyrolyzed via similar conditions vary in char maturity and likely environmental fate.

KEYWORDS: black carbon, pyrogenic organic matter, biochar, FTICR-MS, ^{1}H NMR, dissolved organic matter (DOM)

1. INTRODUCTION

Pyrogenic organic matter (Py-OM) generated via the incomplete combustion of biomass or fossil fuels, is a major carbon component in soils (e.g., Czimczik and Masiello, 2007), is ubiquitous in the atmosphere (e.g., Koch et al., 2009), riverine and ocean waters, and sediments (e.g., Jaffe et al. 2013; Mitra et al., 2002; Coppola et al., 2014), and has important impacts on Earth's carbon cycle and climate. For example, when applied to soils, Py-OM positively impacts soil physicochemical properties and microbial populations, enhancing production, while sequestering carbon from the atmosphere to counteract global climate change (e.g., Lehmann et al., 2008; Lehmann et al., 2011; Gul et al., 2015). In aquatic systems, organismal exposure to Py-OM can produce toxic effects including growth inhibition and death (e.g., Smith et al., 2013), which presumably impacts aquatic ecology. Py-OM applied as biochars also effectively sorb organic pollutants, making them useful for contaminant remediation (e.g., Dai et al., 2019). Global Py-OM production rates are currently poorly known, but a recent estimate of Py-OM produced from vegetation fires (116-385 Tg C y^{-1}; Santín et al., 2016), suggests it has potential to impact carbon cycles at multiple spatial scales. Thus, a better understanding of Py-OM dynamics in the environment is needed.

A major portion of Py-OM often referred to as black carbon and thought to be composed of condensed aromatic compounds (ConAC), has long been assumed to be a slow-cycling insoluble carbonaceous component that persists in soil and sedimentary reservoirs for many thousands of years (e.g., Goldberg, 1985). However, recent research has highlighted that Py-OM and ConAC have soluble components, suggesting they may be more mobile in the environment than previously thought. Laboratory water leaching experiments have demonstrated the release of dissolved Py-OM (Py-DOM) from fresh biochars (Abiven et al., 2011; Mukherjee and

Zimmerman, 2013; Bostick et al., 2018). Further, some portion of insoluble pyrogenic ConAC has been shown to convert to soluble compounds via ozonolysis (Decesari et al., 2002), nitric acid treatment (Kamegawa et al., 1998), and photooxidation (Roebuck et al., 2017), suggesting Py-DOM can be formed via environmental oxidative processes. Multiple studies have demonstrated the presence of water-soluble ConAC in atmospheric (Wozniak et al., 2008; Bao et al., 2017) and aquatic (Hockaday et al., 2006; Ziolkowski et al., 2010; Wagner et al., 2015) environmental samples. Laboratory leachate studies suggest that up to 7% of Py-OM can be mobilized into the Py-DOM pool within the span of a year (e.g., Mukherjee and Zimmerman, 2011; Bostick et al., 2018), and field measurements suggest ConAC may account for as much as 10% of global riverine DOC export (Jaffe et al., 2013). Given the projected increase in wildfires expected to accompany global temperature increases (Scholze et al., 2006) and the increased applications of biochar for agricultural and pollutant remediation purposes (Oliveira et al., 2017), Py-DOM mobilized from Py-OM could be an increasingly important component of future aquatic carbon cycles.

In their recent review of pyrogenic carbon science, Santín et al. (2016) identified several gaps in our understanding of Py-OM cycling including, exchange of Py-DOM between terrestrial and aquatic environments and Py-OM mineralization in soils, sediments, and aquatic systems. Each of these affect the mean residence time of Py-OM in the environment. The ultimate fates of Py-OM (e.g., mobilization, transformation and eventual mineralization, deposition and burial) are tied, in part, to its molecular composition. For example, low molecular weight acids like acetate and formate, found in Py-DOM, are known to fuel heterotrophic respiration (e.g., Wellsbury and Parkes, 1995; Ho et al., 2002). These smaller molecules may comprise the faster cycling components of Py-DOM. Oxygenated aliphatic compounds (H/C > 1.2, O/C >0.5), organic

nitrogen compounds, and compounds with lower molecular weight have all been shown to be both more soluble and more bioavailable than their aromatic and less oxygenated counterparts including ConAC (Ohno et al., 2014). Dissolved ConAC, which are a characteristic component of Py-DOM, are susceptible to complete (to CO_2) and partial photooxidation (e.g., Stubbins et al., 2012; Ward et al., 2014) suggesting their lifetime can be shortened by light exposure.

The long-held assumption is that Py-OM, and by extension Py-DOM, is dominated by ConAC. ^{13}C NMR spectroscopic studies of solid biochars produced at high temperature (>500 °C) show more than 80% contributions from aromatic C (e.g., Bostick et al., 2018). However, Py-DOM made from those biochars has far lower aromatic C (20-37%). And Py-DOM produced from a variety of feedstocks and at a range of temperatures reveal it to contain compounds ranging widely in size and structures (e.g., Smith et al., 2013; Liu et al., 2015; Smith et al., 2016; Fu et al., 2016; Chen et al., 2017). Studies employing electrospray ionization Fourier transform ion cyclotron resonance mass spectrometry (ESI FTICR-MS) identify molecular formulas in Py-DOM consistent with lignin-like, lipid-like, protein-like, and carbohydrate-like compounds in addition to ConAC (Smith et al., 2013; Smith et al., 2016; Chen et al., 2017). Using ^{13}C NMR spectroscopy, Fu et al. (2016) found 15% of freeze-dried bamboo char (400°C) Py-DOM carbon to have aliphatic (CH_2/CH/C) character (versus 50% aromatic). Low molecular weight compounds (e.g., formate, acetate, methanol, propionate, benzene and more) have also been identified as important components of Py-DOM with their relative contribution to the total Py-DOC pool varying widely (e.g., Spokas et al., 2011; Liu et al., 2015; Bostick et al., 2018), as high as 100% for manure and mushroom soil biochars (Spokas et al., 2011).

Recent work has also suggested that Chlorine (Cl) becomes incorporated into biochars during the pyrolysis process. Chlorine has been found to be a significant component in wheat straw-

derived biochar (Joseph et al., 2013). Cl incorporation has been suggested to be the result of volatilized Cl reacting with Py-OM radicals and dependent on pyrolysis temperature with the volatilization of Cl, as HCl, beginning at temperatures less than 200°C and accelerating at 400-500°C (Quyn et al., 2002; Rahim et al., 2012). The polarity of these biochar Cl compounds may contribute to their solubility and make them an important component of the Py-DOM pool.

The observations of a chemically diverse Py-DOM pool would suggest that its fate in the environment may be highly variable. However, studies that systematically compare the chemical compositions of parent feedstock and associated Py-DOM leachate, as a function of biomass type and production temperature are lacking. An understanding of how variations in biochar type influences the chemistry of Py-DOM can help assess Py-DOM potential impact and fate in the environment. Here, we employ FTICR-MS to examine the molecular characteristics of Py-DOM released from oak and grass biochars produced at temperatures ranging from 250°C to 650°C. Py-DOM FTICR-MS data are also compared to additional Py-OM and Py-DOM characterization by complementary techniques (^{1}H NMR spectroscopy, ConAC biomarker analysis) and ^{13}C NMR spectroscopic measurements as reported previously for the same sample set (Bostick et al., 2018).

2. METHODS

2.1 Biochar Production and Py-DOM Isolation.

2.1.1 Biochar Production.

Laurel oak (*Quercus hemisphaerica*, hereafter referred to as Oak) wood and dwarf Fakahatchee grass (*Tripsacum floridanum*, hereafter referred to as Grass) sheaths were used as biomass feedstock for the biochars examined in this study. An oak biochar was produced by

combustion at 250°C (Oak250) in a furnace. All other oak chars were produced by pyrolysis under flowing nitrogen gas at peak temperatures of 400°C (Oak400), 525°C (Oak525), and 650°C (Oak650) held for 3 h. Grass chars were produced under similar pyrolysis conditions at temperatures of 400°C (Grass400) and 650°C (Grass650). The feedstock Oak and Grass biomass are also examined to represent non-pyrolyzed reference materials. Py-DOM was produced from particles ranging 0.25–2.0 mm in size which was obtained by manual crushing and sieving.

2.1.2 Py-DOM Isolation.

Solid Py-OM material was placed in a 250 mL glass flask (pre-combusted at 500 °C, 3 h) with MilliQ water (18.1 MΩ) at a ratio of 1 g solid:40 mL water. The flasks were placed on a shaker table operated at 120 rpm in the dark. The supernatant water was removed from each flask after 24 h, and another 40 mL of MilliQ water was added to the flask for an additional 24 h of agitation on the shaker table. The supernatant was again removed after the second 24 h period, and the two supernatant extracts were combined. The combined supernatants were filtered sequentially through 1.0 μm (Fisherbrand G2 GF/F, pre-combusted at 450 °C) and 0.45 μm (Millipore mixed cellulose ester) filters to isolate Py-DOM. Process blank samples were prepared in the same manner using only MilliQ water (no solid char). Dissolved organic carbon (DOC) concentrations in each extract were obtained using a Shimadzu TOC-V analyzer after acidification to pH~2 with HCl and purging to remove inorganic C. DOC was quantified using a potassium hydrogen phthalate standard curve.

2.2 Solid Py-OM characterization via ^{13}C NMR Spectroscopy.

Biochar solid materials were transferred to a 4 mm rotor covered with a Vespel cap for solid-state ^{13}C NMR analysis using a multiple cross polarization (multiCP) magic angle spinning pulse sequence (Johnson and Schmidt-Rohr, 2014; Hatcher et al., 2018). Experiments were conducted

on a Bruker Avance II spectrometer with ^{1}H resonating at 400MHz and ^{13}C resonating at 100MHz. Samples were spun at the magic angle (54.7°) at a frequency of 14MHz. The continuous pulses were optimized at 0.5 s, and a 0.25 s recycle delay was used. All sample spectra were baseline corrected and calibrated to a glycine external standard (176.03 ppm).

2.3 Py-DOM characterization via FTICR-MS.

2.3.1 Instrumental Analyses.

Py-DOM isolates were solid-phase extracted using PPL cartridges and eluted with methanol following established procedures (Dittmar et al., 2008). The amount of Py-DOM loaded onto each cartridge varied depending on the DOC concentration in each leachate (details provided by Bostick et al., 2018) with the intention of obtaining ~50 mg C L^{-1} (assuming ~50% DOC recovery by the PPL cartridge) in the final eluent. Samples were eluted on the same day they were extracted directly before FTICR-MS analysis to minimize any interactions between methanol and Py-DOM that would transform Py-DOM composition.

Methanol extracts were analyzed by negative ion mode ESI FTICR-MS using an Apollo II ESI source coupled to a Bruker Daltonics 12 T Apex Qe FTICR-MS at the Old Dominion University College of Sciences Major Instrumentation Cluster facility. Samples were infused via a syringe pump into the instrument at a rate of 120 μL h^{-1}. Ions accumulated in the hexapole for 2 seconds prior to transfer to the ICR cell. Exactly 300 transients were co-added for each sample. The summed free induction decay was zero-filled and sine-bell-apodized, then fast Fourier transformed by the Bruker Daltonics Data Analysis software. The methods employed here (PPL extraction, negative ESI FTICR-MS) analyze the portion of the Py-DOM pool that is retained and eluted in methanol after PPL extraction and forms negatively charged ions. Very highly polar molecules that are not retained by the PPL cartridge, low molecular weight molecules

(<300 m/z), and relatively nonpolar Py-DOM molecules are not characterized using this technique.

2.3.2 FTICR-MS Formula Assignments and Classifications.

Mass spectra were calibrated externally with a polyethylene glycol standard and internally using fatty acid and homologous compound series present in each spectrum (Sleighter et al., 2008). Any peaks found in spectra for process blanks were removed from sample mass spectra, as were peaks with signal-to-noise ratios less than 3. Some of the peaks used for calibrations are also identified in process blanks and not assigned to final sample formula lists. Peak m/z values were assigned molecular formulas using the Molecular Formula Calculator from the National High Magnetic Field Laboratory (Tallahassee, FL) and following established molecular formula assignment rules (e.g., Wozniak et al., 2008; Stubbins et al., 2010). Carbon, hydrogen, oxygen, nitrogen, sulfur, phosphorus, and chlorine were considered as potential constituent elements. Formulas containing sulfur and phosphorus are minor components in these char Py-DOM samples (< 1% of spectral signal) and are not considered further. Though Cl is often not assigned to FTICR-MS datasets, isotopic patterns verify Cl assignments. Examination of spectral intensities for ^{35}Cl formulas and their corresponding ^{37}Cl peak (i.e., ~0.32 times the intensity of the ^{35}Cl peak for OM formulas containing 1 Cl) given the natural abundances of ^{35}Cl and ^{37}Cl. Cl 1s XANES spectroscopy (Section 2.4) analyses provide further evidence for organic Cl in Py-OM. Only molecular formulas within an error of ±0.5 ppm were considered. Analytical replicates were performed on selected samples, and peak presence/absence and relative abundance reproducibilities were confirmed following the criteria established in Sleighter et al. (2012).

FTICR-MS, as used in this study, yields information on singly-charged intact ions but cannot give direct structural information. However, molecular formulas can be mined for ratios and metrics that illustrate trends in a sample's predominant compound classes. Molecular formulas are characterized for their H/C and O/C ratios, number of double bond equivalents (DBE), and modified aromaticity index values (AI_{mod}) (Koch and Dittmar, 2006). The DBE is an indication of the degree of unsaturation plus the number of alicyclic structures and is defined as:

$$\mathrm{DBE} = 1 + \mathrm{C} - \frac{\mathrm{H}}{2} + \frac{\mathrm{N}}{2} - \frac{\mathrm{Cl}}{2} + \frac{\mathrm{P}}{2} \qquad \text{(eqn. 1)}$$

The AI_{mod} is an indication of the relative amount of condensed aromatic structures and is defined as follows:

$$\mathrm{AI_{mod}} = \frac{1 + \mathrm{C} - \frac{\mathrm{O}}{2} - \mathrm{S} - \frac{\mathrm{N} + \mathrm{P} + \mathrm{H} + \mathrm{Cl}}{2}}{\mathrm{C} - \frac{\mathrm{O}}{2} - \mathrm{N} - \mathrm{S} - \mathrm{P}} \qquad \text{(eqn. 2)}$$

where C, H, N, Cl, P, O, and S represent the number of carbon, hydrogen, nitrogen, chlorine, phosphorus, oxygen, and sulfur atoms, respectively, in a given molecular formula.

Knowledge of the H/C, O/C, DBE, and AI_{mod} terms for individual molecular formulas, when paired with an understanding of the bonding of natural organic matter, can be exploited further to characterize each formula into logical, operationally-defined compound groups (Fig. S1). Formulas were assigned to one of 9 groups using a modification of the classification system described in previous work (Seidel et al., 2014; Osterholz et al., 2016) such that: 1) saturated fatty acid-like formulas (SFA; $H/C > 2$, $O/C < 0.9$); 2) carbohydrate-like formulas ($O/C > 0.9$, $AI_{mod} \leq 0.5$); 3) unsaturated aliphatic formulas (UA; $1.5 < H/C \leq 2$, N=0, $AI_{mod} \leq 0.5$); 4) peptide-like formulas (Pep; $1.5 < H/C \leq 2$, $N > 0$, $AI_{mod} \leq 0.5$); 5) highly unsaturated aliphatic formulas (HUA) with low oxygen content (HUA low-O; $AI_{mod} \leq 0.5$, $H/C \leq 1.5$, $O/C < 0.5$); 6) highly unsaturated aliphatic formulas with high oxygen content (HUA high-O; $AI_{mod} \leq 0.5$, H/C

≤ 1.5, O/C ≥ 0.5); 7) polyphenolic formulas with low oxygen content (PPh low-O; $0.5 < AI_{mod} \leq 0.66$, O/C < 0.5); 8) polyphenolic formulas with high oxygen content (PPh high-O; $0.5 < AI_{mod} \leq 0.66$, O/C ≥ 0.5); and 9) ConAC formulas ($AI_{mod} > 0.66$).

The ESI FTICR-MS technique as used here is not quantitative due to the competitive nature of the ESI source and the differential ionizability of molecular analytes (e.g., Kujawinski, 2002). However, the comparison of peak magnitudes or intensities has been employed to discern relative compositional differences between samples of similar origin or type that have been handled and analyzed in the same manner (e.g., Sleighter et al., 2012). To facilitate comparison of the Py-DOM samples in this study, molecular formula-derived ratios and metrics (O/C, H/C, DBE, AI_{mod}) and formula classifications are weighted for intensity as follows:

$$X_w = \sum \left(X_i \times \frac{I_i}{I_{tot}} \right) \quad \text{(eqn. 3)}$$

where, X_w is the intensity-weighted mean value for the molecular formula-derived ratio or metric of interest, X_i is the intensity-weighted mean value of the molecular formula-derived ratio or metric of interest for each individual molecular formula *i*, I_i is the spectral intensity of the peak corresponding to each molecular formula *i*, and I_{tot} is the total spectral intensity summed for all assigned molecular formulas. Further, formula group relative abundances were weighted using:

$$\%Y_W = 100 \times \sum \frac{I_Y}{I_{tot}} \quad \text{(eqn. 4)}$$

where $\%Y_w$ is the intensity-weighted percent contribution of the formula group of interest, $\sum I_Y$ is the summed spectral intensity for each molecular formula in the formula group of interest, and I_{tot} is the total spectral intensity summed for all assigned molecular formulas.

2.4. Solid Py-OM characterization via Cl 1s XANES Spectroscopy

Synchrotron-based X-ray absorption near edge structure (XANES) spectroscopy was used to determine Cl speciation in solid biochar materials. Samples were analyzed using beamline 8-BM,

Tender Energy X-ray Absorption Spectroscopy (TES), at the National Synchrotron Light Source II (NSLS II, Brookhaven National Laboratory, Upton, NY). Each sample was mounted onto a halogen-free tape backing as a thin layer of material before being placed into the He filled sample hutch in front of the x-ray beam. All spectra were calibrated against chlorophenol red standard, with its intense π*/σ* transition at 2821.1 eV. Using a 20 x 8 μm incident X-ray beam, fluorescence XANES spectra were collected from 50 eV below to 150 eV above the Cl K-absorption edge with a step size of 0.2 eV around the edge. The dwell time was set to 0.5 sec/point. For each sample, 20 scans were collected (to improve signal to noise) in the same spot and merged into one representative spectrum of the sample. For Oak400, Oak 650, and Grass650 samples, 40 scans were run for each, as these samples had lower Cl fluorescence intensities. Spectra were normalized using Demeter Athena software by fitting a first-order polynomial to the pre-edge region and normalizing the post-edge region to 1.0 by fitting a first- or second-order polynomial depending on the spectral shape. Standard Cl XANES spectra previously collected were used to fit sample spectra using linear combination fitting (LCF) in order to determine the local coordination environment of Cl in each sample and the relative contribution of each Cl bond type in each sample.

2.5 Principal Components Analysis

A principal components analysis (PCA) was performed using the R mseapca package described previously (Yamamoto et al., 2014). Parameters derived from the FTICR-MS Py-DOM data described here as well as ^{1}H NMR, BPCA, and DOC yield data reported in Bostick et al. (2018) were used as input variables (Tables S1-3). Details of the BPCA and ^{1}H NMR analyses can be found in that companion paper (Bostick et al., 2018). In addition to providing principal component (PC) scores and loadings for the samples and variables, respectively, the R

script assesses the significance of variable loadings to PC scores by regressing variable input data to sample PC scores (Benjamini and Hochberg, 1995). The regressions allow calculation of p-values, and variables with p-values <0.05 were considered significant for a given PC.

3. Results and Discussion

3.1 Py-OM Characterization

3.1.1 ^{13}C NMR of Py-OM

The oak and grass biomass and char Py-OM ^{13}C NMR spectra show evidence for the progressive dehydration, decarboxylation, decarbonylation, and aromatization of the original biomass with increasing production temperature as has been observed previously (e.g., Keiluweit et al., 2010; McBeath et al., 2014; Czimczik et al., 2002; Fig. 1). The oak and biomass spectra themselves show features characteristic of these materials as outlined in Table 1. Both biomasses contain features of hemicellulose, cellulose, and lignin with the grass showing higher contributions from peaks indicative of cuticular material (31, 34 ppm) and the oak showing higher contributions of aromatic peaks diagnostic of lignin (132, 149, 155; Fig. 1). The lower temperature chars (250°C, 400°C; Fig. 1) retain some features of the oak and grass biomass spectra (Fig. 1) that are not observed in the higher temperature chars (525°C, 650°C Fig. 1). The NMR peaks characteristic of hemicellulose, cellulose, and lignin (22, 66, 85, 90, 107 ppm, Table 1; e.g., Hedges et al., 1985; Gil and Nieto, 1999) are evident in Oak250, and in Grass400 and Oak 400 to smaller degrees. The retention of biomass signal in Oak250 is consistent with previous thermogravimetric data (Burhenne et al., 2013) which demonstrate biomass loss to begin at pyrolysis temperatures between 200 and 300°C and molecular characterization work that shows the retention of biomass components up to 300°C (Keiluweit et al., 2010). The Oak250

PyOM ^{13}C NMR spectrum shows signal enrichments relative to the oak biomass in a few areas that indicate the initiation of the charring process including: 1) substantially higher relative signal from aromatic carbonaceous material centered at 130-135 ppm, 2) enrichment of methoxy and oxygen-substituted aromatic lignin components at 58 ppm and ~149 ppm relative to the various cellulosic components. These increases in aromatic and lignin-containing components in Oak250 PyOM are consistent with data indicating cellulose and hemicellulose to be more readily decomposed/transformed upon heating relative to lignin (e.g., Burhenne et al., 2013).

At 400°C pyrolysis temperatures, the ^{13}C NMR signal of both the oak and grass char Py-OM, demonstrate a solid material dominated by aromatic signal centered at ~131 ppm with some apparent remnants of biomass components (Fig. 1). Peaks diagnostic of cellulosic and hemicellulosic sources at 66, 85, 90, and 107 ppm are no longer present in either char. Both the Oak400 Py-OM and Grass400 Py-OM retain poorly defined peaks corresponding to the cellulosic methyl peak at ~22 ppm as well as remnants of lignocellulosic oxygenated carbon at ~74 ppm. Notably, the peaks at 22 and 31 ppm in the Grass400 spectrum are much larger than is found for either the Oak250 or the Oak400 chars. This is likely due to the higher contributions of cuticular material in grass relative to wood; cuticular material is primarily located within aerial portions of plants as opposed to internal tissues that dominate the wood pieces charred in our study (Kolattukudy, 1981), found. The carboxyl-C peak at ~170 ppm, the methoxy peak at 58 ppm, and the shoulder peak at 149 ppm corresponding to oxygen-substituted aromatic C are also evident (Fig. 1). Grass400 Py-OM retains more aliphatic (0-45 ppm) and oxygenated (45-110 ppm) features than does Oak400 including a larger apparent methyl peak at 22 ppm, a methylene peak at 31 ppm, and a broadened signal at 74-78 ppm corresponding to hydroxylated C. This suggests a less efficient conversion of grass biomass to ConAC compared to the oak at the 400°C

pyrolysis temperature. Lignin typically represents ~5-10% of grass biomass (e.g., Novaes et al., 2010) but 20-30% of woods (e.g., Pettersen, 1984); as noted earlier, lignin-diagnostic aromatic peaks were more abundant in the oak biomass spectrum. With the lesser lignin content, grass has higher contributions from cellulose and cuticular materials which do not convert to aromatic compounds as efficiently as lignin does.

The ^{13}C NMR spectra of higher temperature char Py-OM (Oak525, Oak650, Grass650) are dominated by aromatic C centered around 128-135 ppm. Using ^{13}C NMR, Bostick et al. (2018) found the aryl-C (110-146 ppm) spectral signal to increase from Oak400 to Oak650 while relative signal assigned to the oxygenated-aryl (146-165 ppm), alkyl (0-110 ppm), and carbonyl (165-220 ppm) groups decreased. Like the oak char trend with temperature, Grass 650 Py-OM shows higher aryl-C and lesser alkyl, oxygenated-aryl, and carbonyl C than Grass 400 Py-OM. Grass400 and Grass650 Py-OM, in comparison to corresponding Oak400 and Oak650 Py-OM, have slightly less relative aryl-C (Grass400: 43% vs. Oak400: 53%; Grass 650: 78% vs. Oak650: 82%) and similar or higher oxygenated aryl-C (Grass400: 15% vs. Oak400: 16%; Grass 650: 9% vs. Oak650: 9%) content. The higher amounts of aryl-C in the oak Py-OM samples relative to grass Py-OM pyrolyzed at the same temperature suggests the oak chars to have reacted to a further extent and to be further along the charring continuum from fresh biomass to turbostratic char. Thus, the chemical composition of the biomass feedstock (i.e., relative lignin, cellulose, cuticle, inorganic content), in addition to its pyrolysis temperature, is an important control on charring extent.

3.1.2 Cl-XANES of Py-OM

Cl-XANES analysis of Py-OM samples reveal much of the Cl in the char samples (up to 22% in grass chars and up to 63% in oak chars) to be organic in form with Oak650 showing the

highest organic content (Table 2). Replicate measurements for Oak650 were quite variable and may reflect the small amount of material characterized in Cl-XANES measurements as opposed to ^{13}C NMR or FTICR-MS which necessarily integrate signal for larger sample sizes. Low volatility organic chlorine compounds are not thought to be abundant in live biomass (<1% by wt.; Bjorkman and Stromberg, 1997; Quyn et al., 2002; Rahim et al., 2012) though aliphatic and aromatic Cl compounds have been identified in senescent plant materials (Myneni, 2002). The presence of organic chlorine in the oak and grass biomass samples may indicate that senescence had begun prior to analysis. Its increased abundance in Py-DOM indicates chlorine may have become incorporated into existing OM during the charring process. Pyrolysis conditions create extremely reactive environments including an abundance of free radical species (e.g., Shafizadeh, 1982; Richter and Howard, 2000), and we suggest that organic compounds react with inorganic chlorine found in plant materials to form the organic chlorine compounds found in our Py-OM samples. The exact mechanisms for chlorine incorporation are likely numerous. One such mechanism may be via radical coupling reactions between chlorine radicals (produced via hydrogen abstraction by organic radicals or heat-induced homolytic cleavage) and organic radicals of several forms (e.g., aromatic, aliphatic, condensed aromatic) (see Supplementary Information Fig. S2, Text S1 for more details). The higher proportion of organic Cl in the Oak650 char further suggests that this process may be enhanced, or that these compounds become concentrated, at higher pyrolysis temperatures. Given the variability in the Oak650 Cl-XANES measurements, future work must examine the range of variability in Cl content within individual Py-OM samples to better understand Cl content along the continuum of Py-OM samples.

The majority of organic Cl in the Py-OM samples was aliphatic in form. Aromatic organic Cl is evident in the high temperature Oak525 and Oak650 chars which have the highest aromatic contents of all Py-OM samples (Fig. 1). The predominance of aliphatic moieties in organic Cl may suggest Cl incorporation into aliphatic molecules to proceed more rapidly than for aromatic compounds.

3.2 Py-DOM FTICR-MS Characterization

3.2.1 Elemental Constituent Overview

The various Py-DOM FTICR-MS analyses reveal a heterogeneous Py-DOM molecular composition (Figs. 2,3,4). Formulas assigned to FTICR-MS spectra of Py-DOM leached from the oak and grass Py-OM samples number between 1,718 (Oak650) and 2,776 (Oak400) (Supplementary Table S1). CHO formulas are the most abundant elemental formula group for all biomass DOM and Py-DOM samples, ranging from 38% (Oak650) to 84% (Oak400) of the spectral intensity of assigned formulas (Fig. 2, Supplementary Table S1). CHON formulas are responsible for the second highest amount of spectral intensity in every sample except for Oak650 Py-DOM, which contained higher relative amounts of CHOCl formulas. N-containing formulas (CHON, CHONCl) represent 1-15% of spectral magnitude with highest contributions in the two 650°C chars, and Cl-containing formulas (CHOCl, CHONCl) account for <1% – 59% of the formula-assigned spectral intensity.

Elemental ratios (O/C, H/C) of the assigned Py-DOM molecular formulas plotted on van Krevelen diagrams (Figs. 3, 4) depict complex DOM mixtures within each char leachate and variable compositions among the chars. Py-DOM molecular formulas are distributed over large O/C (0.05-0.90) and H/C (0.30-2.00) ranges and clearly represent a heterogeneous mixture of compounds in addition to ConAC, the compound class most widely associated with Py-OM and

Py-DOM. These results build upon the growing body of literature that suggest a heterogeneous Py-DOM pool (e.g., Spokas et al., 2011; Smith et al., 2013; Liu et al., 2015; Smith et al., 2016; Chen et al., 2017; Bostick et al., 2018). Each Py-DOM leachate is observed to have a unique distribution of formulas on the van Krevelen diagram. The distinct Py-DOM formula distributions relate to their extent of charring which is dependent on feedstock biomass and temperature of pyrolysis as discussed in the following sections.

Variability in molecular composition may also relate to specific char Py-DOM production conditions unrelated to temperature. Oak and grass chars produced in different 'batches' (i.e., chars produced from biomass prepared and pyrolyzed separately) leach Py-DOM that differ in exact formula distributions and do not meet the criteria for experimental replicates (acceptable replication defined after Sleighter et al., 2012 as >67% formulas in common; Figs. 3, S3, Text S1). Differences in Py-DOM composition between the different batches are pronounced for the Oak char Py-DOM and may relate to inhomogeneities in the wood pieces introduced to the pyrolysis reactor (e.g., size of wood pieces, part of the tree), temperature inhomogeneities within the reactor, or differences in the N_2 flushing rates. Each of these factors likely influence the extent of charring with consequences for Py-DOM composition. A more rigorous examination of the effects of char production conditions and leaching protocols on Py-DOM variability is warranted but beyond the scope of this work. Importantly though, molecular compositions for Py-DOM produced from thermal series of chars follow consistent trends with increasing temperature that facilitate a description of Py-DOM composition based on charring extent. These consistent trends are discussed in detail in the sections that follow.

3.2.2 Oak Py-DOM composition.

The CHO formulas of oak biomass DOM (Fig. 3a) primarily plot in a region of the van Krevelen diagram where one would expect to observe lignin ($0.15 < O/C < 0.6$; $0.5 < H/C < 1.7$) and tannin ($0.6 < O/C < 1.2$; $0.5 < H/C < 1.5$) compounds known to be found in woody material. A cluster of N-containing formulas plot almost exclusively in the area of peptide-like formulas ($0.2 < O/C < 0.5$; $1.5 < H/C < 2.0$). Oak biomass DOM spectral signal is primarily composed of HUA compounds (low-O HUA: 63%, high-O HUA: 15%) with lesser contributions from PPh (low-O PPh: 4%, high-O PPh: 8%), ConAC (5%), and UA (3%) compounds (Figure 5a). The identification of ConAC in biomass-derived leachates is not expected and may reflect the operational definition of ConAC used here ($AI_{mod} > 0.67$) which cannot provide definitive structural confirmation. BPCA analyses on these samples yielded no measurable 5- or 6-ring BPCA compounds indicative of ConAC (Bostick et al., 2018).

The Oak250 Py-DOM shows characteristics of both the initial Oak biomass and the onset of the charring process as is observed for the Py-OM via ^{13}C NMR (Fig. 1). The molecular formulas for Oak250 Py-DOM have the highest mean O/C ratio of all the Py-DOM samples (Fig. 6) along with the highest HUA high-O and PPh high-O contributions of all the Py-DOM samples (Fig. 5a) and an abundance of highly oxygenated ($0.35 < O/C < 0.80$) ConAC formulas (Fig. 3b). Oak250 Py-DOM formulas also show the lowest mean H/C ratio, highest mean number of DBE, and highest mean AI_{mod} value of the oak Py-DOM samples (Fig. 6). The extreme values for these parameters derive from this leachate having the highest PPh high-O and ConAC contributions of all the oak Py-DOM samples (Fig. 5a). Keiluweit et al. (2010) characterize chars produced at < 250°C as transition chars due to incomplete charring. Such chars are composed of biomass that has undergone dehydration and depolymerization of lignin and cellulose components and can be abundant in anhydrous sugars, pyrans, furans, and phenols. Some of these depolymerized lignin

and cellulose components can be observed in the high O/C (O/C > 0.5; HUA high-O, PPh high-O) molecular formulas observed here. The incomplete charring at 250°C also transforms lignin to form well-oxygenated (0.4 < O/C < 0.8) ConAC compounds via a combination of cleavage and volatilization/mineralization of oxygenated alkyl side chains, demethylation of methoxy groups, and radical-mediated condensation of oxygenated aryl compounds (e.g., Knicker et al., 2008; Kim et al., 2014). Oak250 Py-DOM has the highest Py-DOC and ConAC (measured via BPCA) of all the oak chars examined here (Bostick et al., 2018) suggesting that low temperature (250 °C) chars, oak chars in this case, may be major sources of dissolved ConAC to the environment.

With increasing oak char production temperature, Oak Py-DOM mean O/C ratios decrease and H/C ratios increase (Fig. 6). The observed increase in H/C ratio over the temperature continuum is coupled with decreases in mean DBE and AI_{mod}. Corresponding changes are observed in formula classifications over the temperature continuum (Fig. 5a). The relative spectral signal accounted for by UA compounds in oak char Py-DOM increases with char production temperature, and the relative spectral signal accounted for by ConAC, HUA high-O, and PPh high-O compounds decreases (Fig. 5a). Relative spectral signal from CHO formulas in Py-DOM decrease and N-containing and Cl-containing formulas increase in the order Oak400 > Oak525 > Oak650 (Figs. 2, 3c-e). HUA low-O formulas decrease along the same continuum. Oak Py-DOM, thus, becomes less oxygenated and less aromatic as char production temperature increases as determined by ESI FTICR-MS. The decrease in relative oxygen content matches the decrease in solid Py-OM (measured via ^{13}C NMR; Figure 1) and Py-DOM oxygen content (measured by ^{1}H NMR; Bostick et al., 2018) for the same set of samples. Similarly to the oak Py-DOM data here, Smith et al. (2016), examining pinewood chars along a temperature

continuum (300°C, 400°C, 500°C), used FTICR-MS to show a shift to char Py-DOM with higher aliphatic character and lower O/C ratios at higher temperatures. The same study examined pinewood Py-DOM by GC x GC-MS and found various oxygenated compounds (e.g., phenols, acids, furans and ketones, guiacol and pyrocatechol) to be most abundant in 300°C Py-DOM and least abundant in 500°C Py-DOM, while the opposite trend was found for polycyclic aromatic hydrocarbons, compounds that are not observable by ESI-FTICR-MS (Smith et al., 2016). Both oak and pine are woods with abundant lignin components, suggesting the transition from aromatic-dominated to aliphatic-dominated Py-DOM (as detected by ESI-FTICR-MS) with increasing char production temperature may be a characteristic of char Py-DOM from lignin-rich biomasses.

In solid Oak400, Oak525, and Oak650 chars, the wt. %N and N/C ratio in the Py-OM decreases with charring temperature (Bostick et al., 2018). However, the amount of spectral signal accounted for by N- and Cl-containing formulas in Py-DOM increased with charring temperature as did the %N-containing formulas in Py-DOM (Fig. 2). This increase in N-containing molecular formulas from Oak 400 to Oak 525 to Oak 650 could result from soluble N- containing compounds that resist mineralization at higher char production temperatures and become concentrated as CHO compounds are more efficiently mineralized. However, the identities of the N- containing compounds in the Oak Py-DOM samples vary from sample to sample suggesting a dynamic N-containing Py-DOM pool and that specific compounds are not simply resistant to mineralization at higher temperatures. More likely, as pyrolysis temperatures increase, previously insoluble organic N-containing compounds are oxidized and transformed to soluble structures, or inorganic N in the chars resist volatilization and react via free radical

processes during pyrolysis to form N-containing Py-DOM compounds. Either mechanism could explain the apparent concentration of N-containing formulas in high temperature oak Py-DOM.

The same processes may similarly concentrate Cl-containing formulas in higher temperature Py-DOM. Reactions of volatilized Cl and char radical species have been observed in coal and Mallee bark pyrolyzed over similar temperatures with the relative amount of Cl-containing OM a) being dependent on pyrolysis conditions, and b) peaking at a temperature of 600°C (Quyn et al., 2002; Rahim et al., 2012). This peak in Cl-char interactions at 600°C in previous work is consistent with Oak650 Py-DOM having the highest proportion of Cl contribution to molecular formulas. Oak and grass DOM have higher contributions of Cl-containing formulas than some of the Py-DOM samples, however, including Grass650. This suggests that initial charring removes soluble organic chlorine compounds from the dissolved pool, and these Cl-char interactions may be more related to char extent (a factor of temperature and duration of pyrolysis, precursor organic composition, etc.) rather than temperature alone. Thus, we suggest that soluble Cl-containing compounds are formed in the more highly charred samples via reactions of volatilized inorganic Cl with DOM. These chlorinated compounds appear to resist pyrolytic-mineralization relative to CHO compounds. In a wildfire-environment volatilized Cl may escape to the atmosphere more efficiently than in the flowing N_2 gas pyrolysis environment, and the degree to which Cl-incorporation into Py-OM occurs in natural fires requires further research.

Oak Py-DOM N-containing (Py-DON) and Cl-containing formula distributions are like those of the greater Py-DOM pool. Py-DON formulas show decreasing aromaticity and oxygenation with increasing parent char temperatures (Figure 3, 7a). The majority of Oak250 Py-DON formulas are classified as ConAC (referred to as ‘black nitrogen’, 55% of N-containing formula spectral signal) with considerable contributions from PPh high-O (25% of Py-DON formula

spectral signal) and HUA (10% of Py-DON formula spectral signal) formulas and very little signal from formulas resembling peptides (1%). In Py-DOM from chars of higher pyrolysis temperature, N-containing ConAC formula spectral signal (Oak400 = 3%, Oak525 = 15%, Oak650 = 14%) and peptide-like formula spectral signal (Oak400 = 1%, Oak525 = 37%, Oak650 = 33%) both increase suggesting that oak Py-DON bifurcates into aliphatic (peptide-like) and ConAC components.

Cl-containing Py-DOM formulas were found in two locations on the van Krevelen diagram; an oxygenated aliphatic region ($0.25 < O/C < 0.6$; $H/C > 1.5$), and an oxygen-poor aromatic region ($O/C < 0.25$; $H/C < 1$) (Figures 3b,c,d,e, 4b,c). The former group are classified as either UA or peptide-like compounds and were in relatively high abundance (>64% of Cl-containing formula spectral signal) in the oak Py-DOM samples (Figure 3b,c,d,e, 5a) in agreement with the Py-OM Cl-XANES data which characterize most of the organic Cl to be aliphatic in nature (Table 2). Oak650 Py-DOM, derived from the PyOM sample with the highest organic Cl content (Table 2), also contains the highest Cl-containing formula contributions.

The apparent decrease in Py-DOM aromaticity with increasing char production temperature observed via FTICR-MS is in direct contrast to the increases in relative BPCA yield and ^{1}H NMR-derived aromaticity estimated using the same Py-DOM sample series (Fig. 8a; Bostick et al., 2018). Another recent study examining several chars including rice straw, chestnut-wood, and wildfire-derived chars similarly observed negative correlations between total BPCAs and FTICR-MS-derived ConAC compounds (Wagner et al., 2017), suggesting a mismatch between the analytical windows of these two methods. Py-OM has been described to exist on a continuum from slightly charred biomass at low production temperatures to soot at high temperatures (Masiello, 2004). Various Py-DOM measurement techniques are suggested to be better suited for

characterizing Py-DOM components leached from chars along this continuum (Wagner et al., 2018). ESI FTICR-MS may be ill-suited for detecting ConAC derived from soot-type Py-OM due to inefficient ionization of low O/C polycondensed aromatics in the presence of more efficiently ionizable components in the Py-DOM matrix (e.g., oxygenated UA, HUA compounds, chlorinated compounds). As a result, very low O/C, high AI_{mod} compounds in Oak650 Py-DOM may go undetected due to their being outcompeted for charge by more ionizable UA compounds. The extent to which ConAC is present in colloidal size classes (i.e., <0.7 μm but not 'truly dissolved') may also impact dissolved ConAC detection because, for example, ESI-FTICR-MS is not expected to be able to detect colloids whereas BPCA analysis does include colloidal material. Colloidal ConAC may thus result in high BPCA yields not observed via ESI-FTICR-MS. Further work is needed to understand the colloidal versus dissolved nature of biochar-derived ConAC since colloidal material is likely to be less mobile in the environment.

3.2.3 Grass Py-DOM Composition

Grass biomass DOM spectral signal, like oak DOM, is dominated by HUA compounds (low-O = 28%, high-O = 45%) with lesser signal from UA compounds (10%), peptide-like compounds (10%), PPh compounds (low-O = 2%, high-O = 4%), and ConAC compounds (1%) (Figure 5b). The grass biomass DOM sample shows much higher contributions from N and Cl formulas (Fig. 4a) than does the oak DOM (Fig. 3a). The N-containing formulas in the grass biomass DOM are distributed between peptide-like and lignin-like regions of the van Krevelen diagram. This higher N content in grass biomass DOM is consistent with the lower C/N ratios in this material (Bostick et al., 2018). This may reflect the higher protein contents of grasses versus

woody materials (e.g., Bianchi and Canuel, 2011), or differences in the type of lignin in grass versus wood (e.g., Hedges and Mann, 1979).

The relative abundances of chemical components of Grass400 and Grass650 Py-DOM are quite distinct from those for Oak400 and Oak650 Py-DOM, as are compositional trends with production temperature (Figs. 2, 5). The Grass Py-DOM samples show a higher mean intensity weighted O/C ratio (Grass400 = 0.53; Grass650 = 0.51) relative to that observed for the Oak Py-DOM at those temperatures (Oak400 = 0.51; Oak650 = 0.40. Grass400 Py-DOM also has a much higher relative contribution from N-containing formulas (Fig. 2) than Oak400, and both grass Py-DOM samples have considerably smaller relative contributions from Cl-containing formulas. Grass650 Py-DOM character, which is dominated by ConAC and PPh compounds, differs drastically from that of Oak650 Py-DOM, which is predominantly composed of UA compounds. Opposite temperature trends were observed for grass Py-DOM H/C ratio (Grass400 > Grass650), DBE (Grass400 < Grass650), and AI_{mod} (Grass400 < Grass650) compared to Oak Py-DOM (Fig. 3). The Grass400 Py-DOM weighted mean H/C ratio (0.90) is higher, and mean DBE (12.14) and AI_{mod} (0.45) values are lower than those of Grass650 Py-DOM (H/C = 0.67, DBE = 15.03, AImod = 0.62), a result opposite that of the trends observed for the Oak Py-DOM. Similarly, the relative spectral signal of PPh and ConAC increases from Grass400 to Grass650 Py-DOM which is opposite to that observed for the oak char Py-DOM but matches the trend observed for the solid Grass Py-OM ^{13}C NMR and Py-DOM via ^{1}H NMR and BPCA (Fig. 8b).

Similar to oak Py-DON, grass Py-DON formula contributions increase in aromaticity and decrease in relative oxygenation with increasing char temperatures. Grass Py-DON transitions from a majority HUA spectral signal (Grass400: HUA low-O = 29%, HUA high-O = 38% of Py-DON signal) to a majority PPh and ConAC spectral signal (Grass650: PPh low-O = 18%, PPh

high-O = 16%, ConAC = 56% of Py-DON signal) (Fig. 7b). These data suggest that N-containing soluble ConAC are produced at different rates by different biomass sources and at different pyrolysis temperatures, with grass chars showing much higher Py-DON ConAC proportions relative to oak chars. In a study comparing Py-DOM leached from rice straw- and chestnut wood-derived chars (500°C), rice char-derived Py-DOM showed higher relative numbers of ConAC formulas (29% and 17% of all assigned formulas in rice and wood Py-DOM, respectively) and N-containing ConAC formulas (15% and 3% of all assigned formulas in rice and wood Py-DOM, respectively, Wagner et al., 2015). Knicker et al. (2010) suggested that protein-rich biomass, such as grasses, can produce N-rich chars including N-heteroatomic organic matter derived from peptides. The lower lignin and greater protein content in grasses relative to woods, appear to form high temperature (>500°C) chars that leach Py-DOM enriched in oxygenated and N-containing ConAC relative to oak and chestnut woods. Collision-induced dissociation FTICR-MS experiments on N-containing ConAC peaks yielded no losses of N-containing functional groups, suggesting that the N in those compounds are incorporated into polyaromatic cores such as pyrrole, pyridine, pyrazole, or imidazole compounds (Wagner et al., 2015). Nitrogen in such black nitrogen compounds that is incorporated into a polyaromatic core is less likely to be actively recycled into the N pool once deposited to soils or sediments or removed from the aquatic euphotic zone, so this dissolved black nitrogen is thought to be a very slow cycling component of the global N cycle. Grasses may thus contribute disproportionately to the cycling of pyrogenic dissolved organic nitrogen relative to woody biomass.

Chlorine-containing formulas are a very small portion of the grass Py-DOM samples (<5% of spectral signal). Aromatic (including both PPh and ConAC) Py-DOC is typically the dominant form of Cl-containing compound in the grass char Py-DOM (Grass 400: PPh low-O = 26%, PPh

high-O = 0%, ConAC = 45%; Grass 650: PPh low-O = 10%, PPh high-O = 0%, ConAC = 74%; Fig. 7b), which were generally devoid of UA and peptide-like formulas (Figures 4b,c, 5b). This is in apparent disagreement with the Py-OM Cl-XANES data which did not detect aromatic Cl in the solid grass chars. The Cl-XANES technique used here used a microprobe beamline rather than a bulk beam, and it is possible that this difference is indicative of Py-OM sample heterogeneity. It is also possible that the competitive ESI technique preferentially ionized the aliphatic compounds over the aromatic moieties. The aromatic organic chlorine that was observed was primarily composed of compounds that also contained N which may indicate an association between N and Cl within these compounds. Unfortunately, FTICR-MS as used in this study is unable to assess how Cl is bound. Nonetheless, the observation of chlorinated Py-DOM compounds warrant reporting. Future more detailed studies are needed to examine organic Cl concentrations, composition, and formation mechanisms in Py-DOM as well as fate in the environment.

3.2.4 Principal Components Analysis of Py-DOM Composition.

FTICR-MS, ^{1}H NMR, BPCA, and DOC yield data were input into a PCA run for the study DOM and Py-DOM samples in which the first two principal components (PC1 and PC2, respectively) explain 72% of the variability in the dataset (Figure 9, see Table S3 in the supplemental information for input data). PC1 explains 39% of the variability, and sample PC1 scores correlate positively with their FTICR-MS-derived aliphatic and Cl-containing formula characteristics (%UA, %SFA, %CHONCl, %CHOCl, mean H/C ratio, $p<0.05$; Table S4) which have correspondingly high PC1 loadings. Oxygenated and aromatic formula characteristics (%CHO, O/C ratio, AI_{mod}, %PPh-high-O) show very low PC1 variable loadings and sample values that correlate with sample scores ($p<0.05$; Table S4). High DOC yields and relative HUA

high-O formula contributions load positively with PC2 which explaines 33% of the variability in the data. Variables with low PC2 values include BPCA-derived measures of aromaticity (5,6 BPCA, Total BPCA yields, the BACon index), PPh low-O formulas, and low molecular weight compounds identified by ^{1}H NMR.

Beginning with the two biomass samples, the DOM and Py-DOM samples can be traced in a counter-clockwise circle around Fig. 9a to demonstrate changes in Py-DOM with charring extent. The oak and grass biomass samples are most similar to one another due to their high DOC yields (Table S3) and contributions from highly oxygenated HUA formulas (Fig. 5). Oak250 Py-DOM, the sample with the highest mean O/C ratio and %PPh high-O formula contributions and a very high AI_{mod} ratio (Figs. 5,6), has the lowest PC1 score and an intermediate PC2 score. Grass400 Py-DOM has a similarly intermediate PC2 score but a higher PC1 score than Oak250. The biggest differences between these two samples are the lower mean O/C ratio and AI_{mod} observed for Grass400 Py-DOM (Fig. 6) which inform its more positive PC1 score compared to Oak250. Grass650 and Oak400 Py-DOM plot very close to one another in Fig. 9a at intermediate PC1 and the lowest observed PC2 values. These two samples both have high total BPCA yields and contributions from PPh low-O formulas which along with their low DOC yields drives their low PC2 scores (Fig. 5, Table S2). Their similar Py-DOM compositions suggest Grass650 and Oak400 have been charred to similar extents despite the different peak pyrolysis temperatures. The Oak525 and Oak650 Py-DOM samples have increasing PC1 scores due to the high contributions from variables that positively correlate (UA, SFA, and Cl formulas, H/C ratio; Figs. 2, 5, 6) and decreased values for variables that negatively correlate with PC1 (O/C ratio, %CHO formulas; Figs. 2, 6).

3.3 Conceptualization of Py-DOM Composition on a Char Maturity Continuum.

The ^{13}C NMR, FTICR-MS, ^{1}H NMR, and BPCA analyses on these oak and grass Py-OM and Py-DOM samples enhance our conceptual understanding of pyrogenic OM transformations and Py-DOM composition along the char maturity continuum from biomass to low, intermediate, and highly charred OM (Fig. 10). Increased charring decreases Py-OM mass yields and the Py-OM pool becomes increasingly dominated by ConAC with very low O content (e.g., Masiello, 2004; Keiluweit et al., 2010; this study). ^{1}H NMR, BPCA (Bostick et al., 2018), and FTICR-MS (this study) analyses reveal the much smaller Py-DOM pool (~1% of Py-OM) to remain extremely heterogeneous by comparison. Increased charring results in char that produces Py-DOM with both higher aliphatic and aromatic character, a seemingly contradictory result that is made possible by the reduction in oxygenated functionalities. BPCA analyses show the Py-DOM pool to become increasingly enriched in ConAC with increased charring, but these dissolved ConAC contain only 24% of the DOC produced by Oak650 (Bostick et al., 2018). The remaining 76% of the DOC leached from this highly charred Py-OM is made up of a range of compound types containing O, N, and Cl.

The heterogeneity of the Py-DOM pool can be explained in the context of the extremely reactive pyrolytic environment. Pyrolytic reaction systems are driven by organic radicals created by homolytic C-C and C-O bond cleavages (e.g., Kim et al., 2014; Huang et al., 2016). These organic radicals go on to attack and further transform OM via a series of reactions including 1) cleavage of alkyl side chains and functional groups (e.g., decarboxylation, decarbonylation, dehydroxylation, demethoxylation) that produce low molecular weight alkyl compounds, leaving behind a variety of compounds with increased aromaticity and decreased O content, 2) condensation of aromatic rings into ConAC, and 3) ring-opening reactions that produce aliphatic compounds from aromatic compounds (e.g., Huang et al., 2016; Kim et al., 2014; Knicker, 2011;

Zeng, 2000). In the process, much of the OM is mineralized to CO and CO_2, and the remaining Py-OM shows decreased H/C and O/C ratios to a degree dependent on the extent of charring (e.g., Masiello, 2004; Keiluweit et al., 2010). With the losses of oxygen from Py-OM (as CO, CO_2) as pyrolysis progresses along the char maturity continuum, less and less of the Py-OM material has enough polarity to solvate in water, and the Py-DOC yield decreases accordingly. The remaining oxygenated Py-OM components make up most of the Py-DOM pool, and much of this material is the product of side chain cleavages, ring-opening reactions, and radical-driven recombination of these materials.

With progress along the char maturity continuum, the composition of available reactants becomes more aromatic and less oxygenated, and the types of reactions and their products change, with consequences for Py-DOM composition. The cleavage of functional groups is prevalent at all stages of charring shown by abundant low molecular weight oxygenated compounds in chars produced from a diversity of biomasses and at all temperatures (Bostick et al., 2018; Spokas et al., 2011). Cleavage of side chains and fragmentation reactions appear to be most prevalent at low charring extent and continue through intermediate charring when lignocellulosic material is still present. Aromatic condensation reactions also occur at the onset of charring as evidenced by aromatic components in Oak250 Py-OM and Py-DOM. Consequently, the composition of Py-DOM leached from low temperature char is extremely heterogeneous and characterized by HUA, PPh, and ConAC with a wide range of O/C values (0.3-0.9) but a prevalence for high O/C compounds. Any soluble very low O/C ConAC compounds are not likely to be detected by ESI FTICR-MS due to competition for charge but make up a small portion of Py-DOM (Bostick et al., 2018).

At intermediate charring extents, much of the O present in the initial biomass has been removed as CO, CO_2, and volatile oxygenated alkyl compounds. Condensation reactions forming ConAC are therefore expected to increase in relative importance, and ring-opening reactions of the now accumulating ConAC produce aliphatic compounds. Py-DOM from intermediately charred biomass therefore still shows a wide range of O/C ratios (0.3-0.9), but the distribution is balanced between low (O/C < 0.5) and high (O/C > 0.5) oxygen content. HUA, PPh, and ConAC compounds remain the dominant compound groups at intermediate charring, and some aliphatic compounds are formed, presumably from ring-opening reactions.

At high charring extent, Py-OM is largely composed of compounds with low O/C ratios (O/C < 0.5) including an abundance of ConAC of very low O/C (<0.1) that is unobservable by ESI FTICR-MS. Ring-opening reactions become prevalent at high charring extent, resulting in an abundance of aliphatic compounds (e.g., Bostick et al., 2018) which effectively outcompete ConAC for ionization by ESI. Compounds containing N and Cl increase in relative abundance in Py-DOM of this char, suggesting mechanisms that preferentially retain these heteroatomic compounds.

Both biomass species and temperature determine char maturity. Using the characterization scheme described in Figure 10, it is evident that Oak250 can be classified as low maturity chars, Grass400, Oak400, and Grass650 are classified as intermediate maturity chars, and Oak525 and Oak650 are high maturity chars. The reactivity within a pyrolytic system may be accelerated by the presence of inorganic species such as chlorides and transition metals that promote radical reactions and OM transformation, or it can be decelerated by the presence of free radical quenchers. We speculate that the oak pyrolytic system promotes faster progression along the char maturity continuum than the grass pyrolytic system due to some combination of inorganic

pyrolysis accelerants (e.g., Cl radicals) in oak biomass and higher contributions of cuticular material, a potential radical quencher, in grass biomass. Thus, we have determined that Grass650 is of lower char maturity than Oak525 and Oak650.

The two biomass types also yield Py-DOM with different relative contributions from N- and Cl-containing compounds. N-containing formulas are more abundant in grass biomass and intermediate maturity grass chars than in oak biomass and intermediate maturity oak chars. Future work is required to better understand Cl incorporation into char Py-OM and Py-DOM. Here, we demonstrate Cl-containing compounds to be far more abundant in oak than grass Py-DOM and consistent with a process of radical-initiated addition of inorganic Cl to preexisting organic compounds. The greater Cl spectral signal in FTICR-MS analyses of Oak400 and Oak650 Py-DOM relative to Grass400 and Grass650 Py-DOM suggest the oak to either have a higher starting biomass Cl content, its Cl-containing compounds to be more recalcitrant to charring, or to stimulate greater amounts of free radicals during pyrolysis. We speculate that oak pyrolysis generates a greater quantity of free radicals, potentially including Cl-radicals, that accelerate progression along the char maturity continuum, leading to increased spectral signal contributed by Cl-containing formulas and decreased spectral signal contributed by ConAC. The high aromatic content in the oak chars (Fig. 1) may promote halogen addition, and the reactive pyrolysis conditions may then allow for ring-opening reactions producing aliphatic molecules. Unfortunately, neither Cl nor free radicals were quantified in this study, and this speculation will need to be confirmed with future work.

3.4 Methodological Comparison and Considerations

The ESI FTICR-MS technique used in this study cannot characterize the entire Py-DOM pool (or any DOM pool), and the interpretation of Py-DOM FTICR-MS data is best viewed in

the context of several complementary analyses. Some unknown fraction of Py-DOM is lost during the PPL isolation step, and an unknown portion of Py-DOM goes uncharacterized due to charge competition (with inorganic salts or highly ionizable OM components) in the negative electrospray ionization. As a result, ESI FTICR-MS can provide data that are in apparent disagreement with other techniques (Fig. 8). The paired ^{1}H NMR and BPCA analyses suggest that ESI FTICR-MS characterizes a progressively smaller portion of the Py-DOM pool with increasing progression along the char maturity continuum.

When interpreted appropriately and viewed in the context of other measurements, ESI FTICR-MS provides powerful insights that provide a fuller picture of Py-DOM composition. For example, the apparent diminution in oak Py-DOM aromaticity with increasing char production temperature observed via FTICR-MS is in direct contrast to the increases in BPCA yield and ^{1}H NMR-derived aromaticity estimated from the same Py-DOM samples (Fig. 8; Bostick et al., 2018). Without the data from BPCA and ^{1}H NMR analyses, the presence of low O/C, high AI_{mod} compounds in Oak650 Py-DOM would have gone undetected due to their being outcompeted for charge by more ionizable UA compounds. The ESI FTICR-MS data described here add more detailed insights not provided by the BPCA and ^{1}H NMR analyses. FTICR-MS analyses reveal the O/C ratio of Py-DOM compounds to decrease and the relative contributions from N and Cl compounds to increase along the char maturity continuum. Further, the molecular formula information enables characterization of transitions in the HUA, PPh, ConAC, and UA compound groups that would otherwise not been able to be observed. In sum, the multi-proxy approach provides a fuller picture of the apparent Py-DOM molecular composition and is recommended for future Py-DOM characterization studies.

4. Conclusions, Implications for environmental cycling of Py-DOM, and Recommendations for future work

This study undertakes a systematic comparison of the chemistry of biochar leachates generated from chars of different temperatures and feedstocks. The study design incorporated multiple measurement techniques enabling a more complete picture of Py-DOM composition. The results, thus, advance our understanding of Py-DOM composition and cycling by adding important molecular-level details to an existing understanding that had described Py-DOM based mainly on its relative aromaticity. What results is an improved conceptualization of Py-DOM composition on a continuum of char extent. Furthermore, this work provides novel and valuable observations of chlorine incorporation into Py-DOM and information on nitrogenous components of Py-DOM along the char extent continuum.

Py-DOM released upon exposure to water proves to be extremely heterogeneous both in terms of elemental content and molecular distribution. An important conclusion from this work is that Py-DOM composition does not necessarily match the chemical composition of its Py-OM precursor nor is it primarily composed of ConAC. In fact, at the highest char extents, aliphatic compounds are an important component of Py-DOM not easily observed in Py-OM measurements. This new observation results from our study design which examined chars produced at higher char extents than previous Py-DOM studies. The composition of Py-DOM leached from a char relates to its position on a char maturity continuum which depends on both parent solid pyrolysis temperature, the chemical composition of the feedstock material, and perhaps, additional pyrolysis methodological considerations. Py-DOM released from lightly charred materials contain a diverse suite of compounds ranging widely in relative O/C content and aromaticity including low molecular weight compounds, ConAC, and remnant

lignocellulosic material. With increased extent of charring, Py-DOM composition remains diverse but trends at the highest charring extents toward reduced oxygen content and a bifurcation into high aromaticity ConAC and low aromaticity unsaturated aliphatic compounds.

Both oak and grass biomass produce Py-OM and Py-DOM that follow the trends with char maturity described above, but their molecular characters differ in important and previously unrecognized ways. Under the same pyrolysis temperatures, oak chars have higher char maturity due to, we speculate, greater radical reactivity caused by the higher relative amounts of lignin and potential inorganic accelerants in hardwoods and/or the presence of radical quenchers such as cuticular material in grasses. Future work should examine potential factors for differences in charring extent including mineral and lignin content. The higher proteinaceous content of grasses leads to higher apparent nitrogen contributions in grass Py-DOM relative to oak. Oak Py-DOM has significantly higher contributions from Cl-containing compounds. Further work should be conducted to examine whether these trends are species-specific or extend to whole biomass classes (e.g., grasses versus hardwoods).

The compositional heterogeneity and trends with char extent described here for Py-DOM have implications for the mobility and fate of pyrogenic materials produced in wildfires. Py-DOM released from low-temperature lignin-rich hardwoods and protein-rich biomass (e.g., grasses) are likely to be relatively more important sources of Py-DOC (Bostick et al., 2018) and dissolved ConAC to aquatic systems on a mass basis than other chars. These Py-DOM types also contain N-compounds with ConAC character that may be important sources of refractory 'dissolved black nitrogen' to the environment. Chlorinated organics often possess antimicrobial qualities (e.g., Gray et al., 2013), and the high apparent Cl contributions to oak char Py-DOM may render these compounds resistant to breakdown. Conversely, each of the Py-DOM samples

examined here contains abundant contributions from methanol, acetic acid, and formic acid that may represent a bioavailable Py-DOM component. In a wildfire environment, multiple biomass types will experience a range of fire temperatures, durations, and chemical environments, and the extent to which biochar-based work can be extended to understand wildfire Py-DOM is unclear, suggesting the need for well-planned simulated wildfire experiments.

Finally, this work demonstrates the advantage of utilizing multiple analytical tools for characterizing Py-DOM. The ESI FTICR-MS, ^{1}H NMR, and BPCA techniques provide a complementary set of tools for evaluating the nature of Py-DOM composition. Used in isolation, these techniques have been clearly shown in this work to provide an incomplete view of Py-DOM composition. Future studies should continue to employ multiple techniques to more fully understand this heterogeneous material. Future work must also examine methodological influences on Py-DOM composition due to biomass preparation (size of biomass pieces, portion of a tree), temperature and gas flow inhomogeneities in pyrolysis reactors, and Py-DOM isolation protocols (e.g., filter pore size, water to char leaching ratios, effects of sequential leachates). Evaluation of Py-OM production and Py-DOM isolation protocols will be important for understanding how well laboratory studies using biochars represent environmental conditions for biochars and for wildfires.

ACKNOWLEDGMENTS

This work was funded by the U.S. National Science Foundation - Geobiology and Low-Temperature Geochemistry Program (EAR-1451452) and the ODU Frank Batten Endowment Fund. This research used beamline 8-BM (Tender Energy X-ray Absorption Spectroscopy, TES) of the National Synchrotron Lightsource II, a U.S. Department of Energy (DOE) Office of

Science User Facility operated for the DOE Office of Science by Brookhaven National Laboratory under contract No. DE-SC0012704. The authors thank the ODU COSMIC facility as well as Isaiah Ruhl and Jim Hall for assistance with FTICR-MS and NMR analyses. We additionally thank Drs. Rachel L. Sleighter and Hongmei Chen for assistance with FTICR-MS data processing and Dr. Alina Ebling for statistical assistance. Lastly, we thank Dr. Jason Curtis for assistance with elemental analyses, and Dow Van Arnam for the construction and maintenance of the pyrolysis system.

REFERENCES

Abiven, S., Hengartner, P., Schneider, M.P.W., Singh, N., Schmidt, M.W.I., 2011. Pyrogenic carbon soluble fraction is larger and more aromatic in aged charcoal than in fresh charcoal. Soil Biology &Biochemistry 43, 1615-1617.

Bao, H., Niggemann, J., Luo, L., Dittmar, T. and Kao, S.J., 2017. Aerosols as a source of dissolved black carbon to the ocean. *Nature communications*, *8*(1), p.510.

Benjamini, Y. and Hochberg, Y., 1995. Controlling the false discovery rate: a practical and powerful approach to multiple testing. *Journal of the Royal statistical society: series B (Methodological)*, *57*(1), pp.289-300.

Bianchi, T.S. and Canuel, E.A., 2011. *Chemical biomarkers in aquatic ecosystems*. Princeton University Press.

Björkman, E. and Strömberg, B., 1997. Release of chlorine from biomass at pyrolysis and gasification conditions1. *Energy & Fuels*, *11*(5), pp.1026-1032.

Bostick, K., Zimmerman, A.R., Hatcher, P., Mitra, S. and Wozniak, A., 2018. Production and composition of pyrogenic dissolved organic matter from a logical series of laboratory-generated chars. *Frontiers in Earth Science*, *6*, p.43.

Burhenne, L., Messmer, J., Aicher, T. and Laborie, M.P., 2013. The effect of the biomass components lignin, cellulose and hemicellulose on TGA and fixed bed pyrolysis. *Journal of Analytical and Applied Pyrolysis*, *101*, pp.177-184.

Chen, Z., Luo, L., Xiao, D., Lv, J., Wen, B., Ma, Y. and Zhang, S., 2017. Selected dark sides of biomass-derived biochars as environmental amendments. *Journal of Environmental Sciences*, *54*, pp.13-20.

Coppola, A.I., Ziolkowski, L.A., Masiello, C.A. and Druffel, E.R., 2014. Aged black carbon in marine sediments and sinking particles. *Geophysical Research Letters*, *41*(7), pp.2427-2433.

Czimczik, C.I., Preston, C.M., Schmidt, M.W., Werner, R.A. and Schulze, E.D., 2002. Effects of charring on mass, organic carbon, and stable carbon isotope composition of wood. *Organic Geochemistry*, *33*(11), pp.1207-1223.

Czimczik, C. I., & Masiello, C. a. (2007). Controls on black carbon storage in soils. *Global Biogeochemical Cycles*, *21*(3), 1–8. https://doi.org/10.1029/2006GB002798

Dai, Y., Zhang, N., Xing, C., Cui, Q. and Sun, Q., 2019. The adsorption, regeneration and engineering applications of biochar for removal organic pollutants: a review. *Chemosphere*.

Decesari, S., Facchini, M.C., Matta, E., Mircea, M., Fuzzi, S., Chughtai, A.R., Smith, D.M., 2002. Water soluble organic compounds formed by oxidation of soot. Atmospheric Environment 36, 1827-1832.

Dittmar, T., Koch, B., Hertkorn, N. and Kattner, G., 2008. A simple and efficient method for the solid-phase extraction of dissolved organic matter (SPE-DOM) from seawater. *Limnology and Oceanography: Methods*, *6*(6), pp.230-235.

Fu, H., Liu, H., Mao, J., Chu, W., Li, Q., Alvarez, P.J., Qu, X. and Zhu, D., 2016. Photochemistry of dissolved black carbon released from biochar: reactive oxygen species generation and phototransformation. *Environmental science & technology*, *50*(3), pp.1218-1226.

Gil, A.M. and Neto, C.P., 1999. Solid-state NMR studies of wood and other lignocellulosic materials. In *Annual reports on NMR spectroscopy* (Vol. 37, pp. 75-117). Academic Press.

Goldberg, E.D., 1985. *Black carbon in the environment: properties and distribution*. New York: J. Wiley.

Gray, M.J., Wholey, W.Y. and Jakob, U., 2013. Bacterial responses to reactive chlorine species. *Annual review of microbiology*, *67*, pp.141-160.

Gul, S., Whalen, J.K., Thomas, B.W., Sachdeva, V. and Deng, H., 2015. Physico-chemical properties and microbial responses in biochar-amended soils: mechanisms and future directions. *Agriculture, Ecosystems & Environment*, *206*, pp.46-59.

Hedges, J.I. and Mann, D.C., 1979. The characterization of plant tissues by their lignin oxidation products. *Geochimica et Cosmochimica Acta*, *43*(11), pp.1803-1807.

Hedges, J.I., Cowie, G.L., Ertel, J.R., Barbour, R.J. and Hatcher, P.G., 1985. Degradation of carbohydrates and lignins in buried woods. *Geochimica et Cosmochimica Acta*, *49*(3), pp.701-711.

Ho, T.Y., Scranton, M.I., Taylor, G.T., Varela, R., Thunell, R.C. and Muller-Karger, F., 2002. Acetate cycling in the water column of the Cariaco Basin: seasonal and vertical variability and implication for carbon cycling. *Limnology and Oceanography*, *47*(4), pp.1119-1128.

Hockaday, W.C., Grannas, A.M., Kim, S., Hatcher, P.G., 2006. Direct molecular evidence for the degradation and mobility of black carbon in soils from ultrahigh-resolution mass spectral analysis of dissolved organic matter from a fire-impacted forest soil. Organic Geochemistry 37, 501-510.

Huang, J., He, C., Pan, G. and Tong, H., 2016. A theoretical research on pyrolysis reactions mechanism of coumarone-contained lignin model compound. *Computational and Theoretical Chemistry*, *1091*, pp.92-98.

Jacobson, M.Z., 2001. Strong radiative heating due to the mixing state of black carbon in atmospheric aerosols. *Nature*, *409*(6821), p.695.

Jaffé, R., Ding, Y., Niggemann, J., Vähätalo, A.V., Stubbins, A., Spencer, R.G., Campbell, J. and Dittmar, T., 2013. Global charcoal mobilization from soils via dissolution and riverine transport to the oceans. *Science*, *340*(6130), pp.345-347.

Joseph, S., Graber, E.R., Chia, C., Munroe, P., Donne, S., Thomas, T., Nielsen, S., Marjo, C., Rutlidge, H., Pan, G.X. and Li, L., 2013. Shifting paradigms: development of high-efficiency biochar fertilizers based on nano-structures and soluble components. *Carbon Management*, *4*(3), pp.323-343.

Kamegawa, K., Nishikubo, K. and Yoshida, H., 1998. Oxidative degradation of carbon blacks with nitric acid (I)—Changes in pore and crystallographic structures. *Carbon*, *36*(4), pp.433-441.

Keiluweit, M., Nico, P.S., Johnson, M.G. and Kleber, M., 2010. Dynamic molecular structure of plant biomass-derived black carbon (biochar). *Environmental science & technology*, *44*(4), pp.1247-1253.

Kim, K.H., Bai, X. and Brown, R.C., 2014. Pyrolysis mechanisms of methoxy substituted α-O-4 lignin dimeric model compounds and detection of free radicals using electron paramagnetic resonance analysis. *Journal of analytical and applied pyrolysis*, *110*, pp.254-263.

Knicker, H., Hilscher, A., González-Vila, F.J. and Almendros, G., 2008. A new conceptual model for the structural properties of char produced during vegetation fires. *Organic Geochemistry*, *39*(8), pp.935-939.

Knicker, H., 2010. "Black nitrogen"–an important fraction in determining the recalcitrance of charcoal. *Organic Geochemistry*, *41*(9), pp.947-950.

Knicker, H., 2011. Pyrogenic organic matter in soil: Its origin and occurrence, its chemistry and survival in soil environments. *Quaternary International*, *243*(2), pp.251-263.

Koch, B.P. and Dittmar, T., 2006. From mass to structure: An aromaticity index for high-resolution mass data of natural organic matter. *Rapid communications in mass spectrometry*, *20*(5), pp.926-932.

Koch, D., Schulz, M., Kinne, S., McNaughton, C., Spackman, J.R., Balkanski, Y., Bauer, S., Berntsen, T., Bond, T.C., Boucher, O. and Chin, M., 2009. Evaluation of black carbon estimations in global aerosol models. *Atmospheric Chemistry and Physics*, *9*(22), pp.9001-9026.

Kolattukudy, P.T., 1981. Structure, biosynthesis, and biodegradation of cutin and suberin. *Annual Review of Plant Physiology*, *32*(1), pp.539-567.

Kujawinski, E.B., 2002. Electrospray ionization Fourier transform ion cyclotron resonance mass spectrometry (ESI FT-ICR MS): characterization of complex environmental mixtures. *Environmental Forensics*, *3*(3-4), pp.207-216.

Lehmann, J., Skjemstad, J., Sohi, S., Carter, J., Barson, M., Falloon, P., Coleman, K., Woodbury, P. and Krull, E., 2008. Australian climate–carbon cycle feedback reduced by soil black carbon. *Nature Geoscience*, *1*(12), p.832.

Lehmann, J., Rillig, M.C., Thies, J., Masiello, C.A., Hockaday, W.C. and Crowley, D., 2011. Biochar effects on soil biota–a review. *Soil biology and biochemistry*, *43*(9), pp.1812-1836.

Liu, P., Ptacek, C.J., Blowes, D.W., Berti, W.R. and Landis, R.C., 2015. Aqueous leaching of organic acids and dissolved organic carbon from various biochars prepared at different temperatures. *Journal of environmental quality*, *44*(2), pp.684-695.

Masiello, C.A., 2004. New directions in black carbon organic geochemistry. *Marine Chemistry*, *92*(1-4), pp.201-213.

McBeath, A.V., Smernik, R.J., Krull, E.S. and Lehmann, J., 2014. The influence of feedstock and production temperature on biochar carbon chemistry: a solid-state 13C NMR study. *Biomass and Bioenergy*, *60*, pp.121-129.

Mitra, S., Bianchi, T.S., McKee, B.A. and Sutula, M., 2002. Black carbon from the Mississippi River: Quantities, sources, and potential implications for the global carbon cycle. *Environmental science & technology*, *36*(11), pp.2296-2302.

Mukherjee, A., Zimmerman, A.R., Harris, W., 2011. Surface chemistry variations among a series of laboratory-produced biochars. Geoderma 163, 247-255.

Mukherjee, A., Zimmerman, A.R., 2013. Organic carbon and nutrient release from a range of laboratory-produced biochars and biochar-soil mixtures. Geoderma 193, 122-130.

Myneni, S.C., 2002. Formation of stable chlorinated hydrocarbons in weathering plant material. *Science*, *295*(5557), pp.1039-1041.

Novaes, E., Kirst, M., Chiang, V., Winter-Sederoff, H. and Sederoff, R., 2010. Lignin and biomass: a negative correlation for wood formation and lignin content in trees. *Plant Physiology*, *154*(2), pp.555-561.

Ohno, T., Parr, T.B., Gruselle, M.C.I., Fernandez, I.J., Sleighter, R.L. and Hatcher, P.G., 2014. Molecular composition and biodegradability of soil organic matter: a case study comparing two new England forest types. *Environmental science & technology*, *48*(13), pp.7229-7236.

Oliveira, F.R., Patel, A.K., Jaisi, D.P., Adhikari, S., Lu, H. and Khanal, S.K., 2017. Environmental application of biochar: Current status and perspectives. *Bioresource technology*, *246*, pp.110-122.

Osterholz, H., Kirchman, D.L., Niggemann, J. and Dittmar, T., 2016. Environmental drivers of dissolved organic matter molecular composition in the Delaware Estuary. *Frontiers in Earth Science*, *4*, p.95.

Pettersen, R.C., 1984. The chemical composition of wood. *The chemistry of solid wood*, *207*, pp.57-126.

Quyn, D.M., Wu, H. and Li, C.Z., 2002. Volatilisation and catalytic effects of alkali and alkaline earth metallic species during the pyrolysis and gasification of Victorian brown coal. Part I. Volatilisation of Na and Cl from a set of NaCl-loaded samples. *Fuel*, *81*(2), pp.143-149.

Rahim, M.U., Gao, X., Garcia-Perez, M., Li, Y. and Wu, H., 2012. Release of chlorine during mallee bark pyrolysis. *Energy & Fuels*, *27*(1), pp.310-317.

Richter, H. and Howard, J.B., 2000. Formation of polycyclic aromatic hydrocarbons and their growth to soot—a review of chemical reaction pathways. *Progress in Energy and Combustion science*, *26*(4-6), pp.565-608.

Roebuck Jr, J.A., Podgorksi, D.C., Wagner, S. and Jaffé, R., 2017. Photodissolution of charcoal and fire-impacted soil as a potential source of dissolved black carbon in aquatic environments. *Organic Geochemistry*, *112*, pp.16-21.

Santin, C., Doerr, S.H., Kane, E.S., Masiello, C.A., Ohlson, M., de la Rosa, J.M., Preston, C.M. and Dittmar, T., 2016. Towards a global assessment of pyrogenic carbon from vegetation fires. *Global Change Biology*, *22*(1), pp.76-91.

Scholze, M., Knorr, W., Arnell, N.W. and Prentice, I.C., 2006. A climate-change risk analysis for world ecosystems. *Proceedings of the National Academy of Sciences*, *103*(35), pp.13116-13120.

Seidel, M., Beck, M., Riedel, T., Waska, H., Suryaputra, I.G., Schnetger, B., Niggemann, J., Simon, M. and Dittmar, T., 2014. Biogeochemistry of dissolved organic matter in an anoxic intertidal creek bank. *Geochimica et Cosmochimica Acta*, *140*, pp.418-434.

Shafizadeh, F., 1982. Introduction to pyrolysis of biomass. *Journal of analytical and applied pyrolysis*, *3*(4), pp.283-305.

Sleighter, R.L. and Hatcher, P.G., 2008. Molecular characterization of dissolved organic matter (DOM) along a river to ocean transect of the lower Chesapeake Bay by ultrahigh resolution electrospray ionization Fourier transform ion cyclotron resonance mass spectrometry. *Marine chemistry*, *110*(3-4), pp.140-152.

Sleighter, R.L., Chen, H., Wozniak, A.S., Willoughby, A.S., Caricasole, P. and Hatcher, P.G., 2012. Establishing a measure of reproducibility of ultrahigh-resolution mass spectra for complex mixtures of natural organic matter. *Analytical chemistry*, *84*(21), pp.9184-9191.

Smith, C.R., Sleighter, R.L., Hatcher, P.G. and Lee, J.W., 2013. Molecular characterization of inhibiting biochar water-extractable substances using electrospray ionization fourier transform ion cyclotron resonance mass spectrometry. *Environmental science & technology*, *47*(23), pp.13294-13302.

Smith, C.R., Hatcher, P.G., Kumar, S. and Lee, J.W., 2016. Investigation into the sources of biochar water-soluble organic compounds and their potential toxicity on aquatic microorganisms. *ACS Sustainable Chemistry & Engineering*, *4*(5), pp.2550-2558.

Spokas, K.A., Novak, J.M., Stewart, C.E., Cantrell, K.B., Uchimiya, M., DuSaire, M.G. and Ro, K.S., 2011. Qualitative analysis of volatile organic compounds on biochar. *Chemosphere*, *85*(5), pp.869-882.

Stubbins, A., Niggemann, J., Dittmar, T., 2012. Photo-lability of deep ocean dissolved black carbon. Biogeosciences 9, 1661-1670.

Stubbins, A., Spencer, R.G.M., Chen, H.M., Hatcher, P.G., Mopper, K., Hernes, P.J., Mwamba, V.L., Mangangu, A.M., Wabakanghanzi, J.N., Six, J., 2010. Illuminated darkness: Molecular signatures of Congo River dissolved organic matter and its photochemical alteration as revealed by ultrahigh precision mass spectrometry. Limnol. Oceanogr. 55, 1467-1477.

Wagner, S., Ding, Y. and Jaffé, R., 2017. A new perspective on the apparent solubility of dissolved black carbon. *Frontiers in Earth Science*, *5*, p.75.

Wagner, S., Dittmar, T. and Jaffé, R., 2015. Molecular characterization of dissolved black nitrogen via electrospray ionization Fourier transform ion cyclotron resonance mass spectrometry. *Organic geochemistry*, *79*, pp.21-30.

Wagner, S., Jaffé, R. and Stubbins, A., 2018. Dissolved black carbon in aquatic ecosystems. *Limnology and Oceanography Letters*, *3*(3), pp.168-185.

Ward, C.P., Sleighter, R.L., Hatcher, P.G., Cory, R.M., 2014. Insights into the complete and partial photooxidation of black carbon in surface waters. Environmental science. Processes & impacts 16, 721-731.

Wellsbury, P. and Parkes, R.J., 1995. Acetate bioavailability and turnover in an estuarine sediment. *FEMS Microbiology Ecology*, *17*(2), pp.85-94.

Wozniak, A., Bauer, J., Sleighter, R., Dickhut, R., Hatcher, P., 2008. Technical Note: Molecular characterization of aerosol-derived water soluble organic carbon using ultrahigh resolution electrospray ionization Fourier transform ion cyclotron resonance mass spectrometry. Atmospheric Chemistry & Physics 8, 5099–5111.

Yamamoto, H., Fujimori, T., Sato, H., Ishikawa, G., Kami, K. and Ohashi, Y., 2014. Statistical hypothesis testing of factor loading in principal component analysis and its application to metabolite set enrichment analysis. *BMC bioinformatics*, *15*(1), p.51.

Zeng, Y.U., Hong, P.A. and Wavrek, D.A., 2000a. Chemical–biological treatment of pyrene. *Water Research*, *34*(4), pp.1157-1172.

Ziolkowski, L.A., Druffel, E.R.M., 2010. Aged black carbon identified in marine dissolved organic carbon. Geophysical Research Letters 37.

Table 1. Chemical shift assignments for peaks observed in Py-OM ^{13}C NMR data. See text and Figures 1, 2 for more information.

^{13}C NMR Chemical Shift (ppm)	Functional Group Assignment
22	-C-**C**H_3 in acetyl groups of hemicellulose.
31, 34	-C-**C**H_2-CR methylene C in aliphatics including resins such as cuticles in grass
45	α-**C** in peptides
57, 58	-O-**C**H_3 methoxy C in lignin
66	C-**C**H_2OH C_6 in cellulose and hemicellulose
72, 74	-**C**-OR oxygenated aliphatic chains in lignin, cellulose ($C_{2,3,5}$). 72 and 74 peaks indicate amorphous and crystalline cellulose, respectively
85	-C-**C**HOH-C C_4 in cellulose and hemicellulose
90	-**C**HOH C_4 in cellulose and hemicellulose
107	-C-CH(O**C**)$_2$ anomeric C_1 carbon in cellulose or $C_{2,4}$ in lignin
128, 129, 131, 132	Non-oxygen-substituted aromatic carbon in lignin (and char)
149, 153, 155	Oxygen-substituted aromatic carbon in lignin (and char)
170, 174	-C-**C**O_2R or -**C**OOH in lignin and hemicellulose

Table 2. Relative content of Cl detected in solid Py-OM samples via Cl-NEXAFS and in Py-DOM leachates as % FTICR-MS spectral signal.

Sample	% Aliphatic Organic Cl	% Aromatic Organic Cl	% Inorganic Cl	% FTICR-MS Spectral Signal
Oak Biomass	10	7	84	5.7
Oak250	16	0	81	0.4
$Oak400_a$	21	0	79	1.6
$Oak400_b$	19	0	80	1.6
Oak525	9	1	89	14.0
$Oak650_a$	57	6	37	58.8
$Oak650_b$	17	0	82	58.8
Grass Biomass	8	7	86	9.8
Grass400	3	0	97	0.6
Grass650	19	0	78	3.3

Figure Captions

*Figure 1. Figure 1. MultiCP ^{13}C NMR spectra for oak (a) and grass (b) biomass and biochar samples prepared at different pyrolysis temperatures. Numbers indicate chemical shifts corresponding to carbon assignments noted in the text and Table 1.

Figure 2. Relative FTICR-MS spectral signal accounted for a) CHO formulas, b) N-containing formulas (CHON, CHONCl), and c) Cl-containing formulas (CHOCl, CHONCl) for biomass DOM and Py-DOM leachates of biochars produced at the temperatures noted. Note that grass samples were not prepared at 250°C and 525°C. *Note the difference in the y-axis scales*.

*Figure 3. van Krevelen plots of the O/C and H/C ratios for molecular formulas assigned to the leachates of a) Oak biomass, and the biochars of b) Oak250, c) Oak400, d) Oak525, e) Oak650. Data are color-coded for elemental composition as described in panel a.

*Figure 4. van Krevelen plots of the O/C and H/C ratios for molecular formulas assigned to the a) Grass biomass DOM, b) Grass400 Py-DOM, c) Grass650 Py-DOM. Data are color-coded for elemental composition as described in panel a.

*Figure 5. Relative FTICR-MS spectral signal of selected compound groups for the a) Oak Biomass DOM and oak char Py-DOM samples, and b) Grass biomass and grass char Py-DOM samples. The key lists formula group abbreviations as follows SFA = saturated fatty acid-like formulas, UA = unsaturated aliphatic formulas, Carb-like = carbohydrate-like formulas, Peptide-like = peptide-like formulas, HUA low-O = highly unsaturated aliphatic formulas (O/C < 0.5), HUA high-O = highly unsaturated aliphatic formulas (O/C ≥ 0.5), PPh low-O = polyphenolic formulas (O/C < 0.5), PPh high-O = polyphenolic formulas (O/C ≥ 0.5), ConAC = condensed aromatic compound formulas.

Figure 6. Mean a) O/C ratios, b) H/C ratios, c) numbers of double bond equivalents, and d) modified aromaticity index value (AI_{mod}) weighted for spectral magnitude for biomass DOM and Py-DOM leachates of biochars produced at the temperatures noted. X denotes that there is no grass sample at the indicated temperature.

*Figure 7. Relative spectral signal of compound groups for the a) N-containing (% of assigned N-containing formulas) and b) Cl-containing (% of assigned Cl-containing formulas) Oak and Grass biomass and Py-DOM samples. The key lists formula group abbreviations as follows SFA = saturated fatty acid-like formulas, UA = unsaturated aliphatic formulas, Carb-like = carbohydrate-like formulas, Peptide-like = peptide-like formulas, HUA low-O = highly unsaturated aliphatic formulas (O/C < 0.5), HUA high-O = highly unsaturated aliphatic formulas (O/C ≥ 0.5), PPh low-O = polyphenolic formulas (O/C < 0.5), PPh high-O = polyphenolic formulas (O/C ≥ 0.5), ConAC = condensed aromatic compound formulas.

*Figure 8. Measures of Py-DOM aromatic content made by different analytical methods for a) Oak Biomass DOM and char Py-DOM and b) Grass Biomass DOM and char Py-DOM. Gray and black bars represent PPh and ConAC formula spectral signal, respectively (left axis), from FTICR-MS analyses. Blue dots represent ^{1}H NMR relative aromatic spectral signal (adjusted for estimated C content, left axis), and orange dots represent Total BPCAs (mg BPCA/g DOC, right axis) from Bostick et al (2018).

Figure 9. Principal component analysis PC1 vs. PC2 biplots of a) study DOM and Py-DOM sample scores and b) FTICR-MS, BPCA, DOC, and ^{1}H NMR variable loadings. Variable loadings that correlate with PC1 or PC2 ($p<0.05$) are labeled in panel b.

*Figure 10. Trends in Py-OM and Py-DOM yield and composition along a char maturity continuum with hotter color and arrows indicating direction of quantitative increase.

*Figures 1, 3-5, 7, 8, 10 should all be printed in color in the final manuscript.

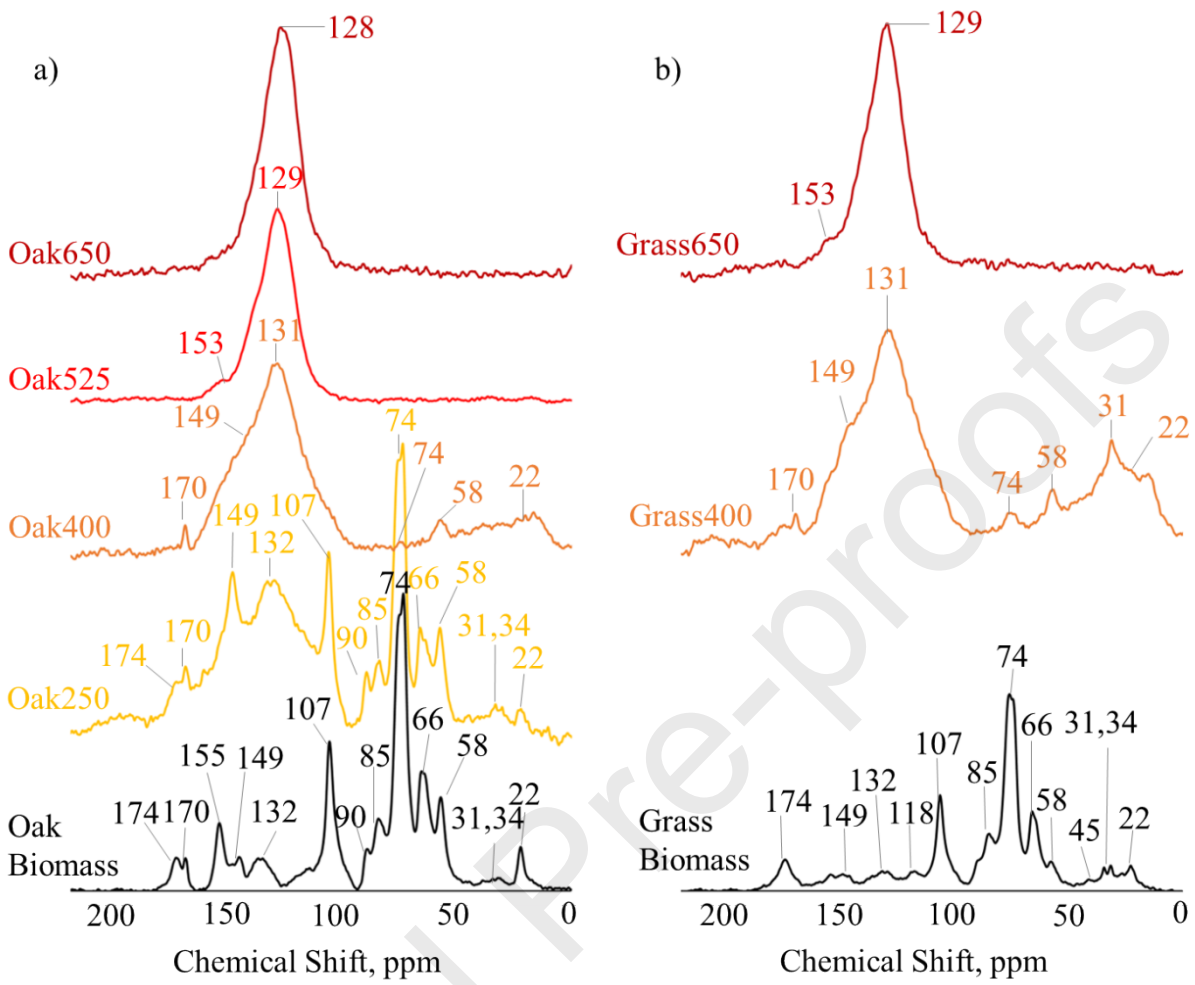

Figure 1. MultiCP ^{13}C NMR spectra for oak (a) and grass (b) biomass and biochar samples prepared at different pyrolysis temperatures. Numbers indicate chemical shifts corresponding to carbon assignments noted in the text and Table 1. Sample spectra and chemical shift labels are color-coded by char temperature (biomass = black, 250 = yellow, 400 = orange, 525 = red, 650 = maroon).

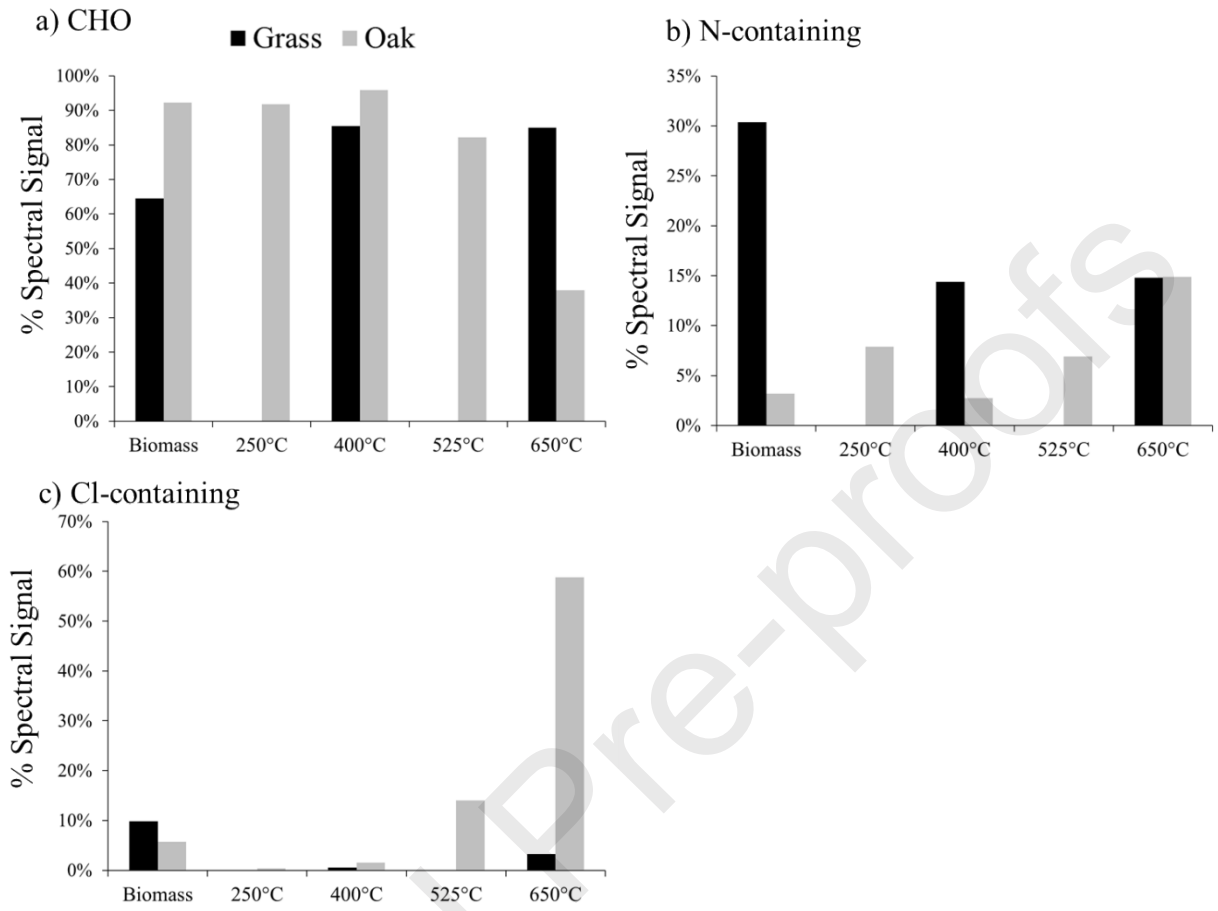

Figure 2. Relative FTICR-MS spectral signal accounted for a) CHO formulas, b) N-containing formulas (CHON, CHONCl), and c) Cl-containing formulas (CHOCl, CHONCl) for biomass DOM and Py-DOM leachates of biochars produced at the temperatures noted. Note that grass samples were not prepared at 250°C and 525°C. *Note the difference in the y-axis scales*.

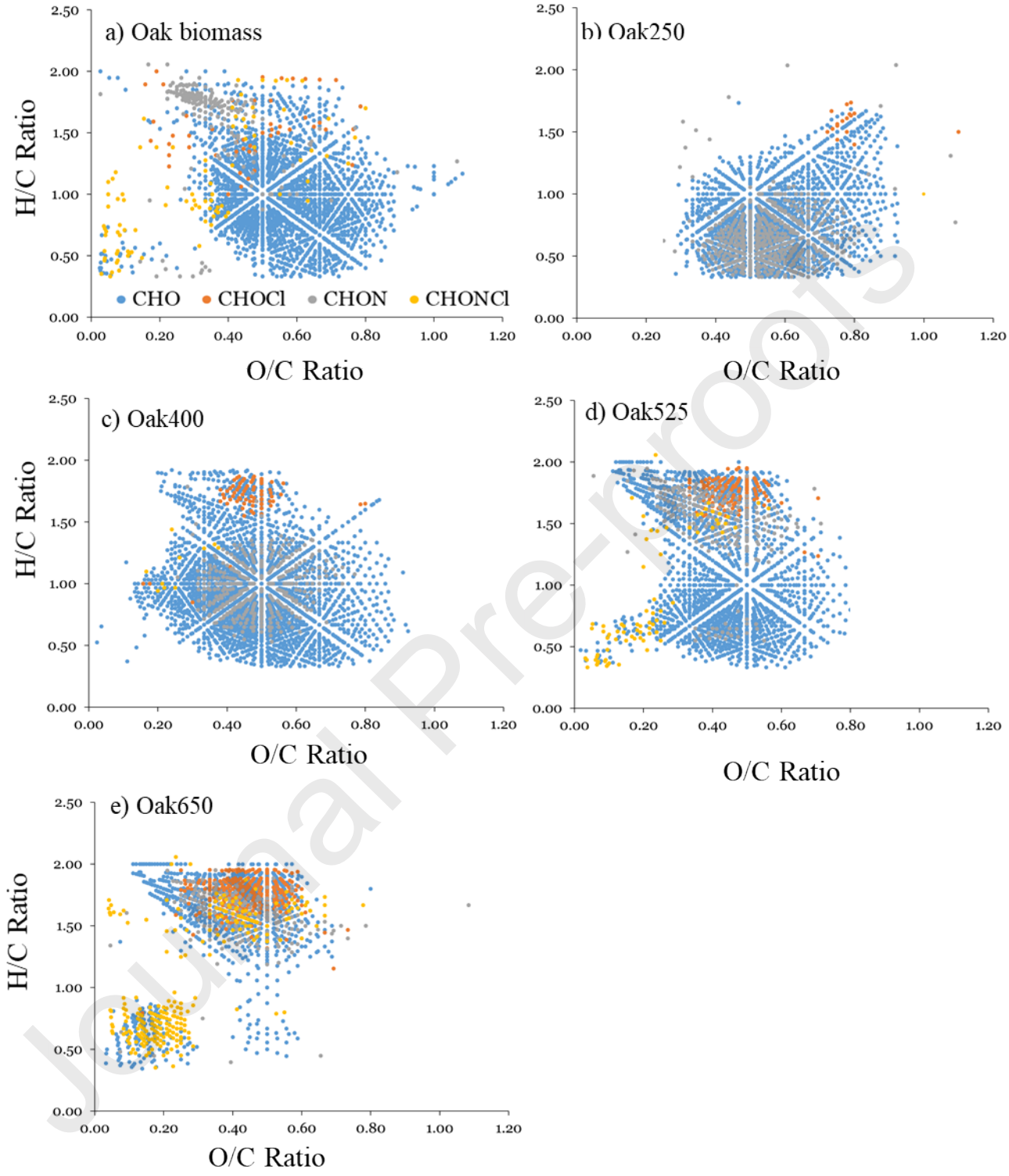

Figure 3. van Krevelen plots of the O/C and H/C ratios for molecular formulas assigned to the leachates of a) Oak biomass, and the biochars of b) Oak250, c) Oak400 , d) Oak525, e) Oak650. Data are color-coded for elemental composition as described in panel a.

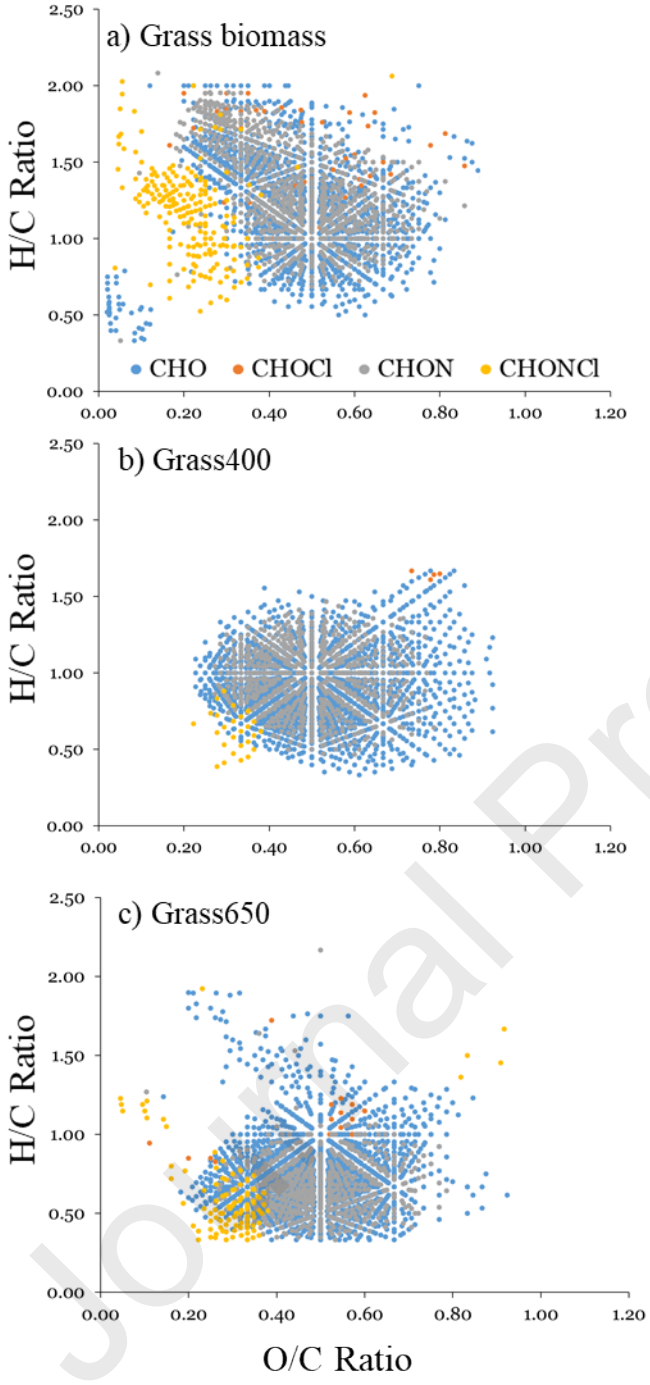

Figure 4. van Krevelen plots of the O/C and H/C ratios for molecular formulas assigned to the a) Grass biomass DOM, b) Grass400 Py-DOM, c) Grass650 Py-DOM. Data are color-coded for elemental composition as described in panel a.

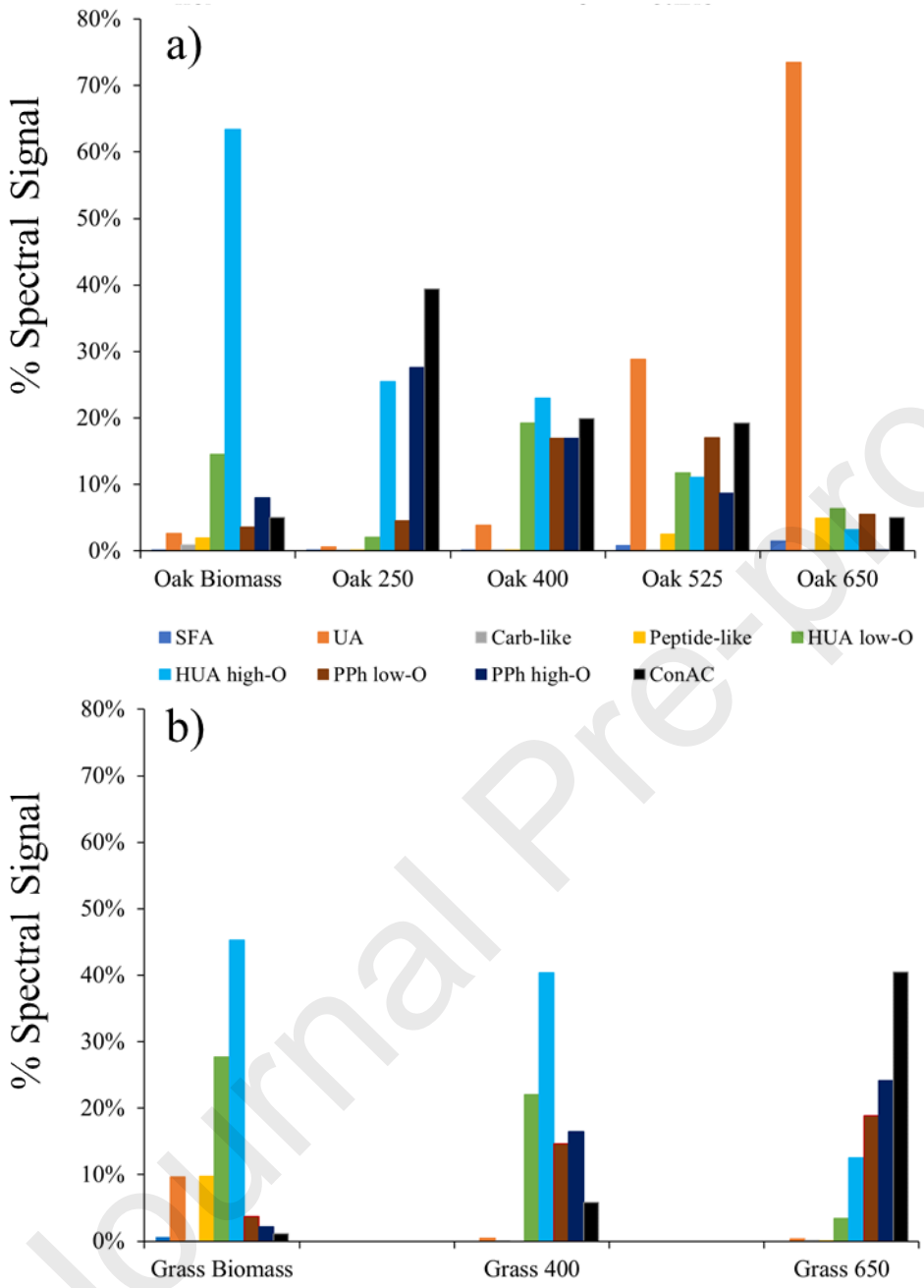

Figure 5. Relative FTICR-MS spectral signal of selected compound groups for the a) Oak Biomass DOM and oak char Py-DOM samples, and b) Grass biomass and grass char Py-DOM samples. The key lists formula group abbreviations as follows SFA = saturated fatty acid-like formulas, UA = unsaturated aliphatic formulas, Carb-like = carbohydrate-like formulas, Peptide-like = peptide-like formulas, HUA low-O = highly unsaturated aliphatic formulas (O/C < 0.5), HUA high-O = highly unsaturated aliphatic formulas (O/C ≥ 0.5), PPh low-O = polyphenolic formulas (O/C < 0.5), PPh high-O = polyphenolic formulas (O/C ≥ 0.5), ConAC = condensed aromatic compound formulas.

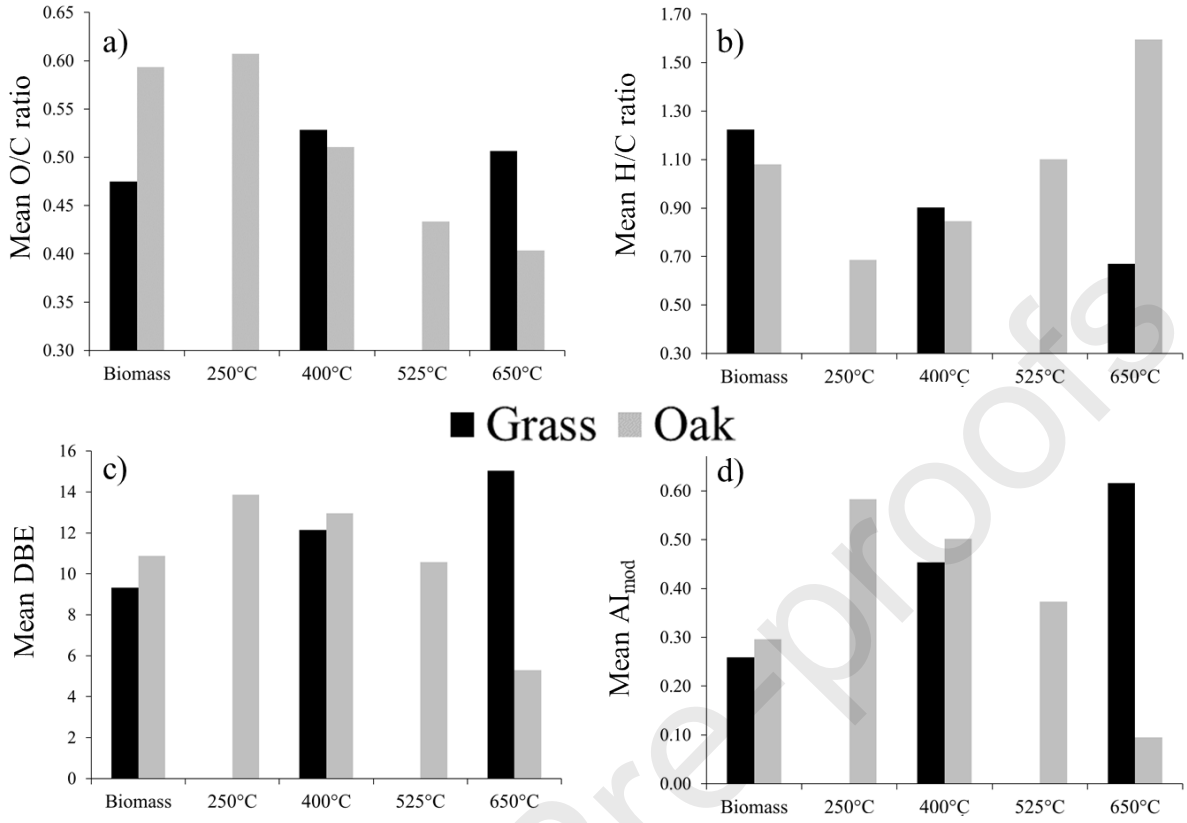

Figure 6. Mean a) O/C ratios, b) H/C ratios, c) numbers of double bond equivalents, and d) modified aromaticity index value (AI_{mod}) weighted for spectral magnitude for biomass DOM and Py-DOM leachates of biochars produced at the temperatures noted. Note that grass samples were not prepared at 250°C and 525°C.

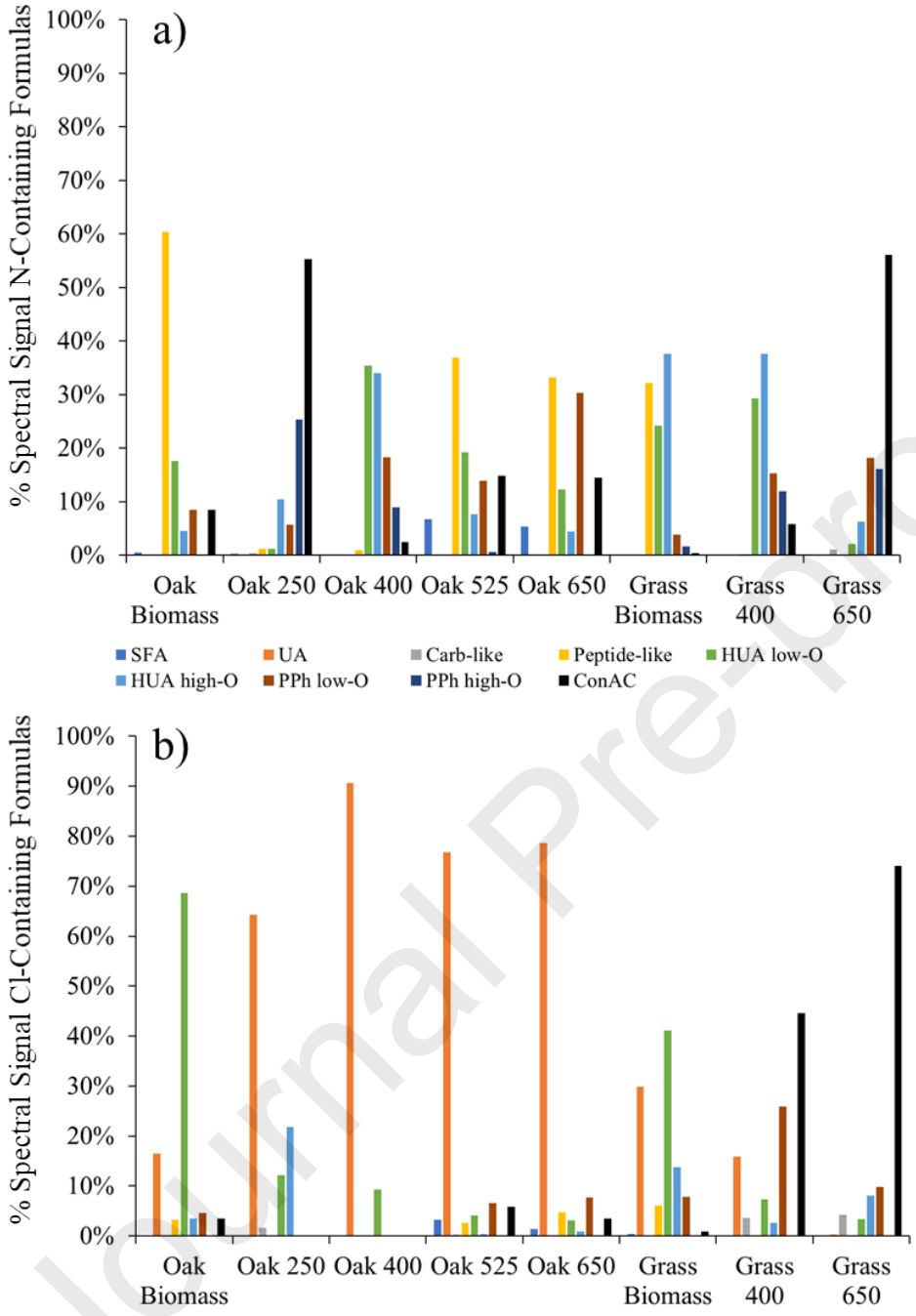

Figure 7. Relative spectral signal of compound groups for the a) N-containing (% of assigned N-containing formulas) and b) Cl-containing (% of assigned Cl-containing formulas) Oak and Grass biomass and Py-DOM samples. The key lists formula group abbreviations as follows SFA = saturated fatty acid-like formulas, UA = unsaturated aliphatic formulas, Carb-like = carbohydrate-like formulas, Peptide-like = peptide-like formulas, HUA low-O = highly unsaturated aliphatic formulas (O/C < 0.5), HUA high-O = highly unsaturated aliphatic formulas (O/C ≥ 0.5), PPh low-O = polyphenolic formulas (O/C < 0.5), PPh high-O = polyphenolic formulas (O/C ≥ 0.5), ConAC = condensed aromatic compound formulas.

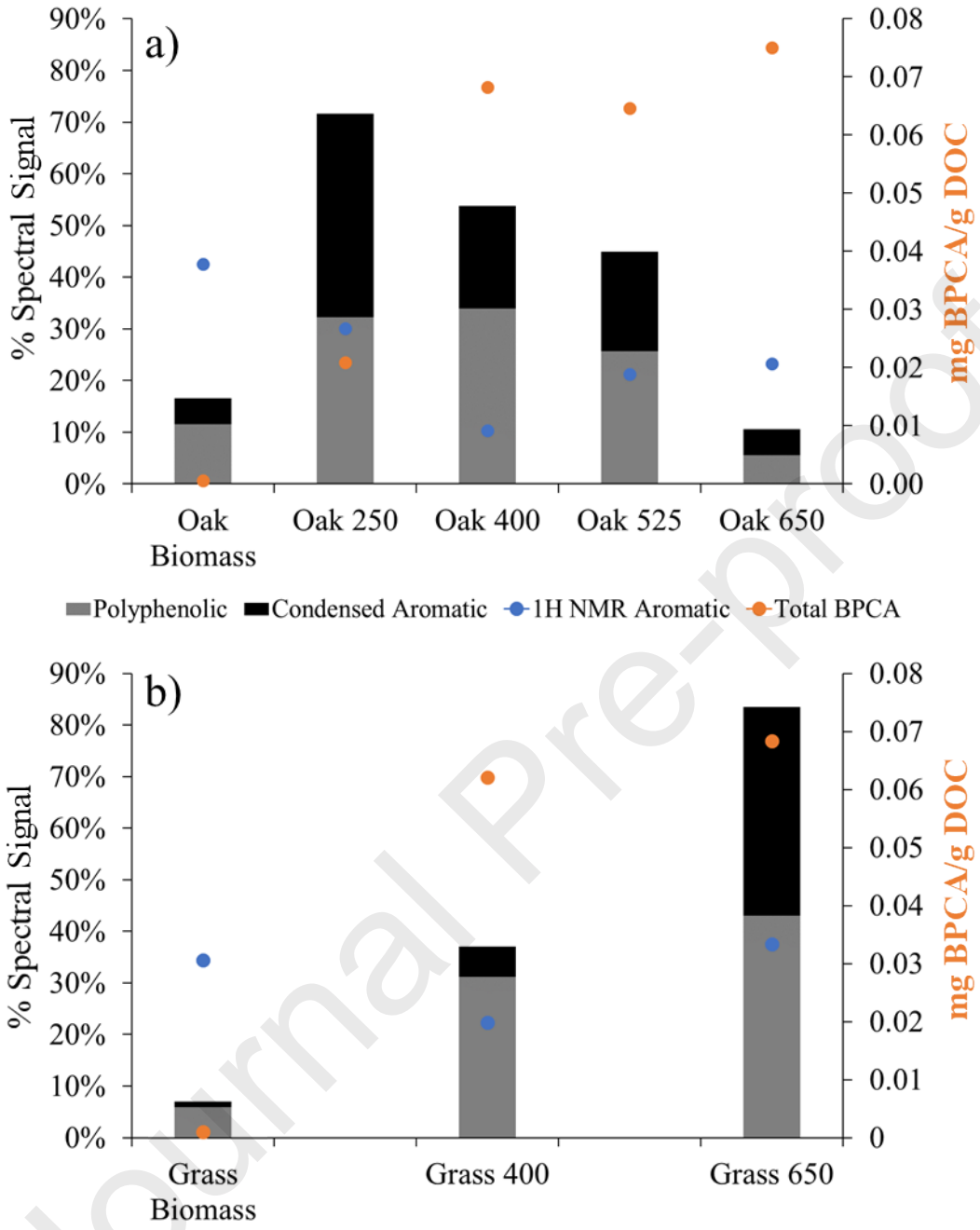

Figure 8. Measures of Py-DOM aromatic content made by different analytical methods for a) Oak Biomass DOM and char Py-DOM and b) Grass Biomass DOM and char Py-DOM. Gray and black bars represent PPh and ConAC formula spectral signal, respectively (left axis), from FTICR-MS analyses. Blue dots represent ^{1}H NMR relative aromatic spectral signal (adjusted for estimated C content, left axis), and orange dots represent Total BPCAs (mg BPCA/g DOC, right axis) from Bostick et al (2018).

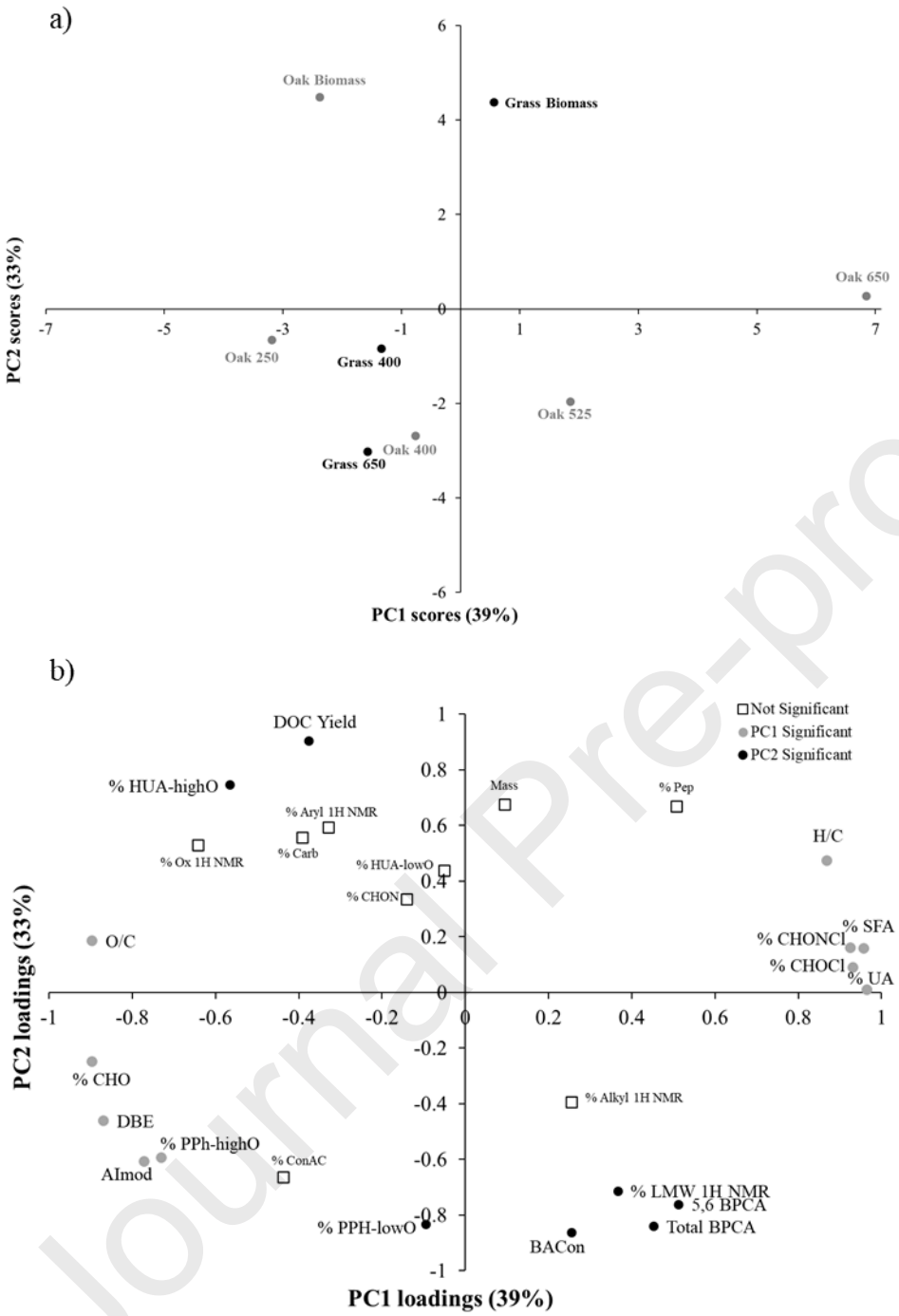

Figure 9. Principal component analysis PC1 vs. PC2 biplots of a) study DOM and Py-DOM sample scores and b) FTICR-MS, BPCA, DOC, and ^{1}H NMR variable loadings.

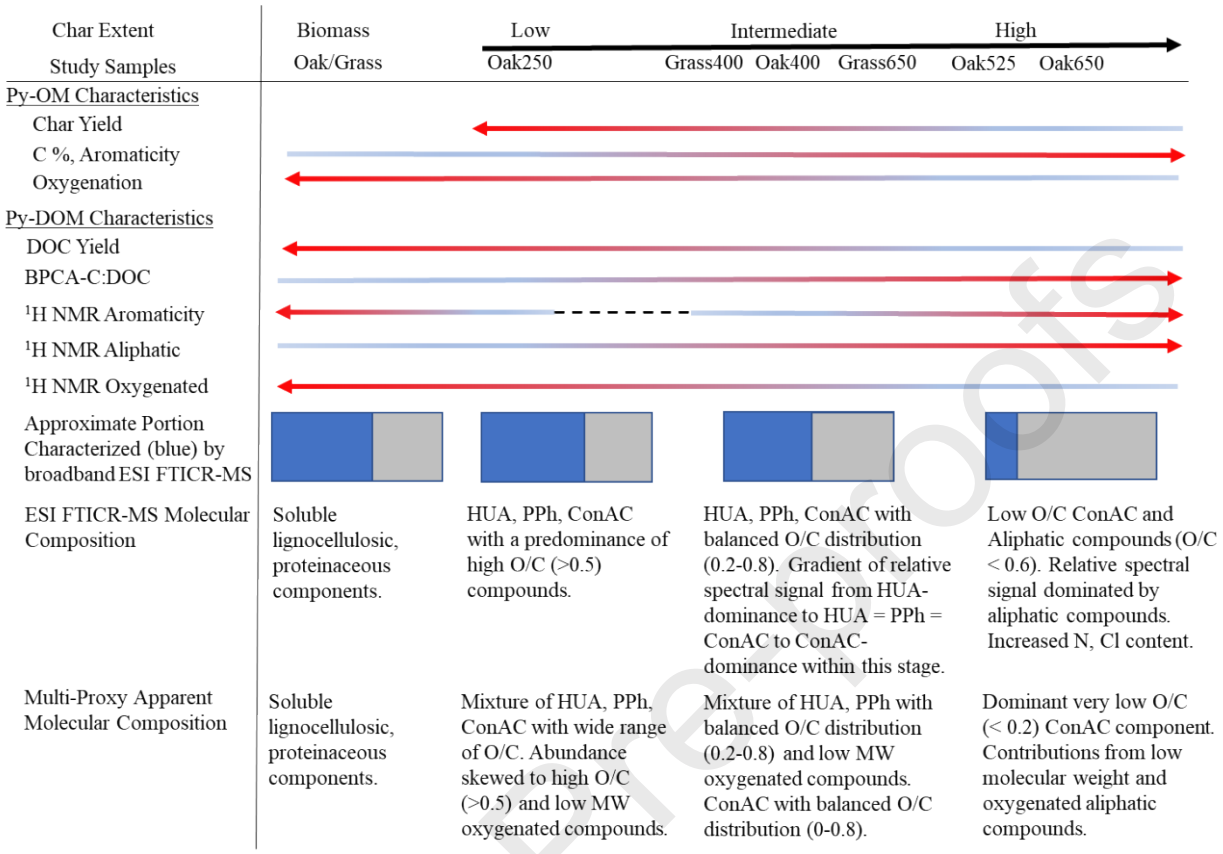

Figure 10. Trends in Py-OM and Py-DOM yield and composition along a char maturity continuum with hotter color and arrows indicating direction of quantitative increase.

Declaration of interests

☒ The authors declare that they have no known competing financial interests or personal relationships that could have appeared to influence the work reported in this paper.

☐The authors declare the following financial interests/personal relationships which may be considered as potential competing interests: